Université de Montréal

Structural Dynamics of the Selectivity Filter in HCN1 Ion Channel

By Sajjad Ahrari

Department of Pharmacology and physiology
Faculty of Medicine
Université de Montréal

Thesis presentation
with a view to obtaining the Master's degree
in Pharmacology

18 May 2020

Université de Montréal

Structural Dynamics of the Selectivity Filter in HCN1 Ion Channel

By Sajjad Ahrari

Has been evaluated by a Jury composed of the following people:

Rafael Najmanovich
Jury President

Nazzareno D'Avanzo
Research Director

Jurgen Sygusch
Jury assessor

18 May 2020

Résumé

Les canaux HCN (cycliques nucléotidiques) activés par hyperpolarisation appartiennent à la superfamille des canaux cationiques voltage-dépendants et sont responsables de la génération de courant drôle (If) dans les cellules cardiaques et neuronales. Malgré la similitude structurelle globale avec le potassium voltage-dépendant (Kv) et les canaux ioniques cycliques nucléotidiques (CNG), ils montrent un modèle de sélectivité distinctif pour les ions K^+ et Na^+. Plus précisément, leur perméabilité accrue aux ions Na^+ est essentielle à son rôle dans la dépolarisation des membranes cellulaires. Ils sont également l'une des seules protéines connues à sélectionner entre les ions Na^+ et Li^+, faisant des HCN des canaux semi-sélectifs. Ici, nous étudions les propriétés de sélectivité uniques des canaux HCN à l'aide de simulations de dynamique moléculaire. Nos simulations suggèrent que le pore HCN1 est très flexible et dilaté par rapport aux canaux Kv et qu'il n'y a qu'un seul site de liaison ionique stable dans le filtre de sélectivité qui les distingue des canaux Kv et CNG. Nous observons également que la coordination et l'hydratation des ions diffèrent dans le filtre de sélectivité de HCN1 par rapport aux canaux Kv et CNG. De plus, la coordination des ions K^+ par les groupes carbonyle du filtre de sélectivité est plus stable par rapport aux ions Na^+ et Li^+, ce qui peut expliquer les propriétés de sélectivité distinctes du canal.

Mots-clés: Canal HCN, Canal ionique, Filtre de sélectivité, Dynamique structurale, Simulation MD, Sélectivité lithium-ion.

Abstract

Hyperpolarization-activated cyclic nucleotide-gated (HCN) channels belong to the voltage-gated cation channel superfamily and are responsible for the generation of funny current (If) in cardiac and neuronal cells. Despite the overall structural similarity to voltage-gated potassium (Kv) and cyclic nucleotide-gated (CNG) ion channels, they show distinctive selectivity pattern for K^+ and Na^+ ions. Specifically, their increased permeability to Na^+ ions is critical to its role in depolarizing cellular membranes. They are also one of the only known proteins to select between Na^+ and Li^+ ions, making HCNs semi-selective channels. Here we investigate the unique selectivity properties of HCN channels using molecular dynamics simulations. Our simulations suggest that the HCN1 pore is very flexible and dilatated compared to Kv channels and that there is only one stable ion binding site within the selectivity filter which discriminates them from both Kv and CNG channels. We also observe that ion co-ordination and hydration differ within the selectivity filter of HCN1 compared to Kv and CNG channels. Additionally, the co-ordination of K^+ ions by the carbonyl groups of the selectivity filter is more stable compared to Na^+ and Li^+ ions, which may explain the channel's distinct selectivity properties.

Keywords: HCN channel, ion channel, selectivity filter, structural dynamics, MD simulation, Lithium ion selectivity.

Table of contents

Résumé 2
Abstract 3
Table of contents 4
List of Figures 6
Abbreviations 7
Acknowledgement 9
Introduction 10
1- Background 11
1.1- HCN channels in health and disease 11
1.1.1- Physiological roles of HCN channels 11
1.1.1.1- HCN channels in the heart 11
1.1.1.2- HCN channels in the central nervous system 15
1.1.2- Disease associate with HCN malfunction 16
1.2- Sequence and structure of HCN channels 18
1.2.1- Family of HCN channels 18
1.2.2- Sequence arrangement of HCN1 channel 20
1.2.3- Structural architecture of HCN channels 21
1.3- Selectivity filter in HCN channels 23
1.3.1- Ion selectivity and permeation in HCN channels 23
1.3.2- Comparing the selectivity in HCN and Kv channels 23
1.3.3- Comparing the selectivity in HCN and CNG channels 26
2- MD simulation for studying ion channels 28
2.1- From electrophysiology to MD simulations 28
2.2- Molecular dynamics simulation to study voltage gated ion channels 29
2.2- Rational for studying ion selectivity in HCN channel by MD simulation 29
3- The idea of Molecular dynamics simulation 30
3.1- Calculating atoms trajectory based on potential energy function 30
3.2- Temperature and pressure control 32

3.3- Periodic boundary conditions 32
3.4- Water molecules 33
3.5- MD simulation package and forcefield 33
4- The manuscript on the structural dynamics of selectivity filter in HCN channel 35
5- Discussion 68
5.1- Dynamics of selectivity filter in HCN1 channel 68
5.2- Ion localization in selectivity filter of HCN1 channel 69
5.3- Network of Hydrogen bonds between selectivity filter and pore helix 70
5.4- Limitations of the study 70
5.4.1- Using the closed conformation of the channel 70
5.4.2- The time period of simulation 71
5.5- Future directions 71
5.5.1- Site-directed mutagenesis studies to manipulate selectivity filter dynamics 71
6- Conclusion 72
7- Bibliography 73

List of Figures

FIGURE 1. ACTION POTENTIAL IN DIFFERENT REGIONS OF HEART [4]. 13

FIGURE 2. ACTION POTENTIAL IN NODAL AND NON-NODAL CELLS OF THE HEART [5]. 14

FIGURE 3. IMPLICATIONS OF PATHOLOGIES OF DYSFUNCTION OF HCN CHANNELS IN CNS AND PNS LISTED BY PRECLINICAL AND CLINICAL STUDIES [21] 18

FIGURE 4. REPRESENTATION OF THE AMINO ACID RELATIONSHIPS OF THE MINIMAL PORE REGIONS OF THE VOLTAGE-GATED ION CHANNEL SUPERFAMILY [2] 19

FIGURE 5. THE TOPOLOGY OF THE HCN CHANNEL SUBUNIT [45]. 21

FIGURE 6. STRUCTURE OF HCN1 CHANNEL [49]. 22

FIGURE 7. AMINO ACID SEQUENCE OF SELECTIVITY FILTER AND PORE HELIX IN HCN, CNG AND KV CHANNELS. THE SEQUENCES OF THE SELECTIVITY FILTER AND PORE HELIX ARE HIGHLIGHTED. SF: SELECTIVITY FILTER. 24

FIGURE 8. THE STRUCTURAL ARRANGEMENT OF SELECTIVITY FILTER RESIDUES IN HCN CHANNEL VERSUS CNG, NAK AND KCSA CHANNELS. 26

FIGURE 9. PHYLOGENETIC TREE AND STRUCTURAL MODEL OF CYCLIC NUCLEOTIDE-REGULATED CATION CHANNELS [61]. 27

FIGURE 10. A SCHEMATIC REPRESENTATION OF THE MOLECULAR DYNAMICS PROCESSES..... 31

Abbreviations

Amino Acid One Letter Code

A Ala Alanine

C Cys Cysteine

D Asp Aspartate

E Glu Glutamate

F Phe Phenylalanine

G Gly Glycine

H His Histidine

I Ile Isoleucine

K Lys Lysine

L Leu Leucine

M Met Methionine

N Asn Asparagine

P Pro Proline

Q Gln Glutamine

R Arg Arginine

S Ser Serine

T Thr Threonine

V Val Valine

W Trp Tryptophan

HCN: Hyperpolarization-activated Cyclic Nucleotide–gated

CNBD: Cyclic Nucleotide Binding Domain

VSD: Voltage Sensor Domain

CNG: Cyclic Nucleotide-gated channels

Kv: Voltage-gated potassium channels

Cav: Voltage-gated calcium channel

cAMP: Cyclic Adenosine Monophosphate

cGMP: Cyclic Guanosine Monophosphate

C-linker: Region connecting the HCN channel to the CNBD

SAN: Sinoatrial Node

AVN: Atrioventricular Node

I_f: Cationic inward current activated by hyperpolarization

I_h: Cationic inward current activated by hyperpolarization

GOF: Gain of Function

LOF: Loss of Function

CNS: Central Nervous System

EPSP: Excitatory Postsynaptic Potential

PFC: Prefrontal Cortex

PNS: Peripheral Nervous System

Cryo-EM: Cryogenic Electron Microscopy

MD simulation: Molecular Dynamics simulation

Ps: Picosiemens (10^{-12} siemens)

fs: Femtosecond (10^{-15} second)

V1/2: Mid-point voltage of activation fitted by Boltzmann function

ECG: Electrocardiogram

KcsA: K channel of streptomyces A

AMBER: Assisted Model Building with Energy Refinement

GROMACS: Groningen Machine for Chemical Simulations

NAMD: Nanoscale Molecular Dynamics

CHRAMM: Chemistry at Harvard Macromolecular Mechanics

OPLS: Optimized Potentials for Liquid Simulations

GROMOS: Groningen Molecular Simulation

VMD: Visual Molecular Dynamics

PDB: Protein Data Bank

Acknowledgement

The journey to a MSc has not been an easy one, but I am extremely grateful for the people around me who have made the trip more enjoyable.

I would like to give my warmest gratitude to Dr. Nazzareno D'Avanzo, for adopting me into the lab, always encouraging me on the path, and helping me finish the degree. There were so many times when I would complain about the projects or the stress, and he was always positive and reassuring of my progress and my abilities.

Thank you to my committee members, Dr. Rafael Najmanovich and Dr. Jurgen Sygusch, for their valuable inputs and for insightful discussions and advice given to me on my Memoire.

I am grateful for the financial support that I received from UdeM and the Natural Sciences and Engineering Research Council of Canada (NSERC).

My time in graduate school was made much more enjoyable by the company of other members of the D'Avanzo laboratory. Thank you for your friendship and enjoyable discussions. A special thanks to Yoann Lussier a former research associate in the lab, that was both a mentor and a confidant on this journey.

Outside of the lab, I interacted with wonderful staff. Specifically, I am grateful to Dr. Rene Cardinal for always being willing to answer my countless questions and inspiring me by his kind advice.

Finally, to my family; I would not have reached this this far without your sincere encouragement and sacrifices. Thank you from the bottom of my heart!

Introduction

Plasma membrane serves as a hydrophobic barrier around the cells and controls receiving the materials from and returning them to the outside environment of cells. These material species include water, ions, amino acids and metabolites. Channels are transmembrane proteins that form a hydrophilic pore and allow for regulated passage of selected species. This passage is tightly regulated to promise the precise permeation of the right substance at a demanded circumstance. Such regulatory mechanism is tightly coupled to a variety of open or close signals such fluctuations in membrane microenvironment of secondary substances which work like a key for opening or closing these gates.

Hyperpolarization-activated cyclic nucleotide-gated (HCN) channels belong to the voltage-gated cation channel superfamily and are responsible for the generation of I_h in cardiac and neuronal cells [1,2]. HCN channels generate pacemaker activity and modulate cellular excitability in the brain and heart. Indeed, in last few years, multiple connections between HCN channels dysfunction and pathological states have been made and HCN has been proposed as a novel target for the treatment of related heart and central/peripheral nervous system disorders. Among the HCN blockers, Ivabradine is an approved drug for the symptomatic management of stable heart-related chest pain and heart failure [3] and several other compounds are being evaluated.

Each of the four protein isoforms are coded by different genes and each isoform is composed of four subunits made up of the same fundamental structural scheme; six alpha helices, which are molded into the structure of the channel transmembrane domain, and two cytosolic domains at the NH and COOH termini [4].

The overall structure of HCN channel is very similar to that of Kv channels; The channel is composed of four identical subunits which are assembled in the membrane to form a 4-fold symmetric pore made by helices S5 through S6. This pore is surrounded by membrane-embedded voltage sensors (helices S1 through S4), similar to Kv channels [5,6]. Despite the overall structural similarity to voltage-gated potassium (Kv) channels, HCNs show much lower selectivity for K^+ over Na^+ ions. Leaking the Na^+ ions at potentials close to that of resting membrane is critical to its role in depolarizing cellular membranes. Besides, they are one of the only known proteins to select between Na^+ and Li^+ ions, making HCN channels semi-selective channels, rather than non-selective like the closely related CNG channels. Differences in selectivity between HCN, CNG and Kv channels has been attributed to the different orientation of selectivity filter residues, which

renders the pore wide-open at the top, resembling a funnel with the first and second binding sites falling apart and unable to coordinate the ions synchronously. However, the 3D arrangement of selectivity filter, cannot explain all the selectivity feature, hence the need to inspect its dynamics in the presence of various cations. Using molecular dynamics simulations, we are investigating the unique selectivity properties of HCN channels. Our simulations suggest that the HCN1 pore is very flexible and dilatated compared to Kv channels and that there is only one stable binding site within the selectivity filter. Additionally, the conserved network of hydrogen bond between the pore helix and selectivity filter only exists for the residues at the bottom of the pore in case of HCN1 channel and is augmented upon C358T mutation.

1- Background

1.1- HCN channels in health and disease

1.1.1- Physiological roles of HCN channels

HCN channels have a $V_{1/2}$ near the typical cell resting membrane potential, and thus their activation or deactivation can occur with only small deviations in voltage. In resting membrane physiological conditions, the activation of HCN channels leads to the net influx of Na^+ ions which in turn triggers membrane depolarization. This influx of Na^+ ions which is accompanied with K^+ ions at hyperpolarized states, produces a current known as funny current (I_f) or hyperpolarization-activated current (I_h) or H-current. The following section outlines several key physiological roles of HCN channels which regulate not only heart and brain function, but also the resting properties of cells within many different organs. Channel opening and closing must be precisely timed and occur at precise voltages to allow for correct tissue function, particularly in the sinoatrial (SA) node of the heart and in neurons. An absence of HCN channels, or channels that do not open and close at the correct instances, can lead to pathological conditions.

1.1.1.1- HCN channels in the heart

The rhythmic and spontaneous nature of cardiac muscle, despite removing the heart from the body indicated that its activity was independent from the nerves [7]. It was initially suggested that regulating this rhythmic firing of action potential in the heart was due to a number of electrical

currents [8] and was thought to be associated with a decaying potassium current observed in Purkinje fibers; Upon depolarization, it was suggested that an outward potassium current (IK2) diminishes as an onset to firing a subsequent action potential. This current seemed to associate with sympathetic innervations of heart rate because it was modulated by β-adrenergic stimulation [9,10]. A decade later, this notion was challenged by the observation that adrenaline increases an inward current in rabbit SAN tissues and in contrast to the IK2 current, this pacemaker current is carried by a mix of sodium and potassium ions and is activated upon hyperpolarization [11]. The pacemaker current is also known as the "funny" current (If) due to its odd and eccentric properties compared to previously well-known potassium, sodium and calcium voltage-activated currents that activate upon membrane depolarization and conduct mainly one ion.

The frequency of a beating heart depends on the rate of diastolic depolarization during an action potential in pacemaker cells of the sinoatrial node. The cardiac impulse originates in the sinus atrial node (SAN), located at the right atrial endocardium (between the upper and lower cava vein). This impulse is formed by highly specialized cells able to generate action potentials that start the sinus rhythm (Fig. 1A). These action potentials in turn allow cardiac muscle cells to contract and make the heart to play its work. The spontaneous and rhythmical contraction of heart muscles is dependent of several internal clocks. HCN channels are among the set of channels responsible for regulating these clocks and have a role in stimulating the cardiac action potential.

According to different phases of actional potential and the channels being involved, the action potential in different cardiac conduction system can be divided into two main categories: non-nodal cells action potential and nodal cells action potential (Fig. 1B) [12]. The nodal cells mainly include sinoatrial (SA) node and the atrioventricular (AV) node. SA node is the normal site for the origin of the action potential that stimulates heart muscle to contract and is located in the upper region of the right atrium. The AV node is specialized for slow conduction of the impulse and to behave as an electrical filter to prevent the ventricles from being paced faster than they can fill with blood (which otherwise can cause an atrial tachyarrhythmia). The non-nodal zones mainly include the His bundle and bundle branches that are specialized for rapid conduction and delivering the wave of action potentials to the inner ventricular myocardium (endocardium) via a web-like network of Purkinje fibers.

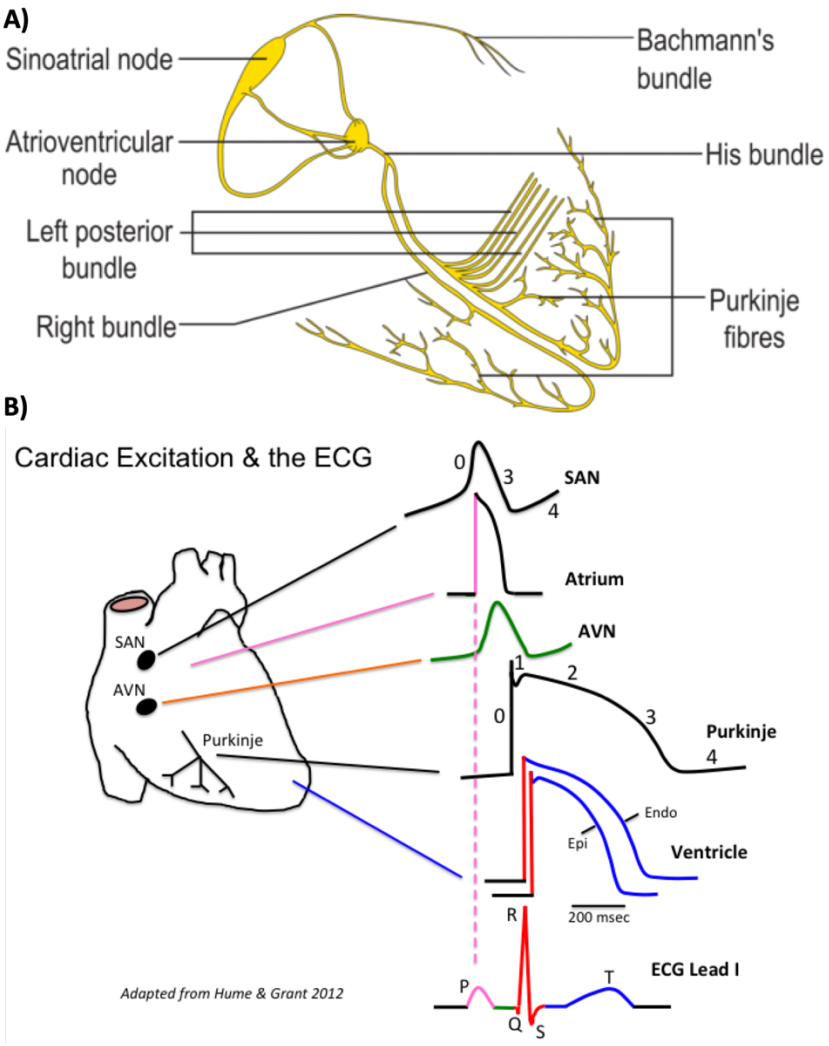

Figure 1. Action potential in different regions of heart [13].

In the latter case, the non-nodal, this process involves 5 steps. First of all, phase 0, corresponds to the rapid depolarization of the membrane via an increase in sodium inward conductance (Na^+) and a decrease in potassium conductance (K^+). During phase 1, potassium channels open and the calcium channels become closed. In the next phase, phase 2, which is also known as plateau phase, the repolarizing effect of potassium channels opening is counterbalanced by activation of the L-type Ca^{++} current upon opening of the calcium channels. As the calcium conductance fades, opening of additional K channels and further outward K^+ currents eventually lead to a phase of rapid repolarization (phase 3). The resting membrane potential is reached at phase 4 and potential remains near the equilibrium potential for K^+. Phase 4 is mainly associated with activation of

potassium channels. The only channel type that opens on a regular basis during this phase is an "inwardly rectifying" K-selective channel which produces a K^+ current called IK1. However, several other channels such as HCNs channels can modulate this phase. For example in Purkinje fibers, activation of HCN channels lead to production of the funny current (I_f) which is produced upon an inward flux of Na^+ ions (that is greater than the efflux of K^+ ions through K channels), leading to the decrease in depolarization threshold and increased excitability of the cells [12-14].

In case of nodal cells, the action potential takes place without phases 1 and 2. In fact these cells do not experience a true resting potential at phase 4. Instead, during this phase the leaking of Na^+ ions through HCN channels (funny currents; I_f) that are partially open at -60mv, slowly increases the membrane potential above and past the action potential threshold. The action potential spikes followed by opening of Ca^{++} channels and membrane depolarization in Phase 0. Phase 3 follows as the repolarization occurs through K^+ channels opening and the outward directed, hyperpolarizing K^+ currents. At the same time, the Ca^{++} channels become inactivated and close (Fig. 2).

The cardiac action potential is therefore a system with two clocks, the clock that is stimulus-driven and depends on Ca^{++} channels (which produce calcium currents of type T and L). the other clock is spontaneous and is mainly regulated by rhythmic opening of the HCN channels and the production of I_f current [12-14].

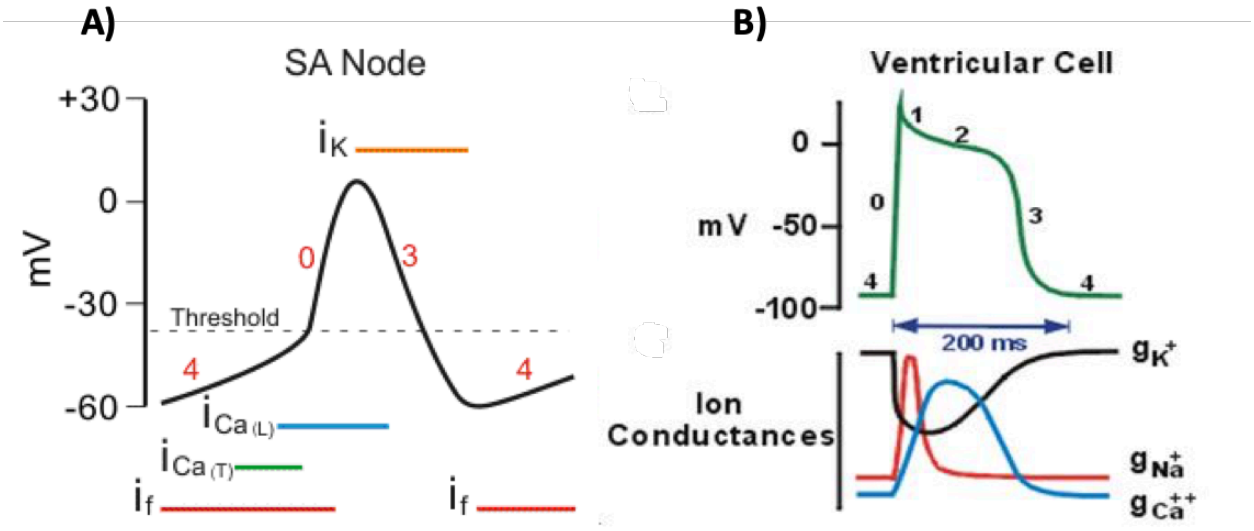

Figure 2. Action potential in nodal and non-nodal cells of the heart [14].

1.1.1.2- HCN channels in the central nervous system

Thus far, four HCN isoforms, HCN1-4, have been cloned [15,16]. These isoforms are diversely spread throughout the central nervous system (CNS), with HCN1 being predominantly present in the cortex, hippocampus, cerebellum and brain stem. HCN2 isoform is mainly situated in areas such as the thalamus and brain stem. HCN3 is expressed at low levels in the CNS whilst HCN4 subunits are highly localised to specific regions such as the olfactory bulb [17,18].

The presence of HCN channels in neurons plays a crucial role in the transmission of signals as well as in controlling the excitement of nerve cells [19,20]. In fact, HCN channel play a dual role in regulating the neurons excitability and triggering the action potential in these cells; by leaking the Na^+ ions at potentials close to -65mV, HCNs increase the excitability of the membrane by maintaining the membrane potential close to its activation potential and can induce a tonic firing pattern of action potential. At the same time, these channels inhibit the membrane from meeting hyperpolarized states by keeping the membrane close to depolarized and exited state. This in turn could interfere with the membrane response to external stimuli which demand a hyperpolarized state of the membrane [19,20].

HCN channels also have a key role in regulating the integration of electrical inputs within neurons; Neuronal dendrites receive excitatory post synaptic potentials (EPSPs) from many synapses all along their length. In order to generate a single sensory output, EPSPs need to be temporally and spatially summed at the soma before propagating down the axon. This process is called dendritic integration [21]. As HCN channels can be open at the resting membrane potential, they can increase membrane conductance. The increasing number of HCNs on the membranes as they extend away from the soma guarantees the inhibition of EPSPs decay due to membrane resistance, as they start being transmitted from distal dendrites [22-24].

HCN channels also have an important role in regulating neuronal excitability through interfering with the process of long-term potentiation (LTP); a frequently used neuronal pathway will develop improved signal transmission. This process is known as LTP and is essential in developing memories [25]. As strong synapses are formed during LTP process, the generation of action potentials through EPSPs are facilitated [26]. LTP thus has the potential to make neurons susceptible to overactivation and generating unnecessary EPSPs. Therefore, the LTP process must be carefully regulated. HCN1 channels inhibit LTP in the hippocampus [27]. Mice with a HCN1 knockout in

forebrain area showed enhanced LTP, as shown by improved performance in spatial memory tasks [28].

Similar to their role in SA cells of the heart, HCN channels help specific network of neurons to beat in an oscillatory and rhythmic pace. For example, the rapid eye movement phase of sleep (REM), require neurons to continuously undergo coordinated oscillations. Additionally, in the non-REM phase of sleep depend on rhythmic "waves" of action potentials within the thalamus that are dispensable of any sensory inputs [29]. These pacemaker-like oscillations can become synchronized between different brain regions to create the electrical activity characteristic of different sleep stages.

HCN channels are also widely expressed in the peripheral nervous system and there is increasing evidence demonstrating a crucial role played by the class of HCN ion channels in starting and controlling firing frequency of action potentials responsible for pain [30]. Specifically, recent findings have shed light on the role of HCN2 isoform in the transmission of pain [31]. Additionally, recent experimental data have highlighted the key role played by HCN2 in both inflammatory and neuropathic pain, suggesting the selective blocking of its activity as a potential target for the treatment of pain. Although the HCN1 isoform is one of the pharmacological targets of the potent and widely used anesthetic propofol [32], its contribution to the transmission of pain seems to be limited.

1.1.2- Disease associate with HCN malfunction

HCN4 is the main isoform associated with heart disease. Here an overview the disease related to central and peripheral nervous system is presented that are often associated with other isoforms of the proteins. These associations are summarized in figure 3 [33].

The association between HCN channels malfunction and epilepsy has been the center of attention since years ago as a molecule called Lamotrigine, which affects HCN channels, showed anti-convulsant results [34]. However, to date there is no evidence that the two (HCN malfunction and epilepsy) have cause and effect relationship. However, modification of the function of HCN channels is clearly potentially able to cause uncontrolled action potential firing and provide a background setting for the development of epilepsy [35]. Additionally, several line of studies suggest

that point mutations altering HCN1 channel function are poorly tolerated and predispose neurons to hyperexcitability, but may not be sufficient by themselves to cause seizure development [36-38].

The modulation of HCNs channels also has been suspected to have indirect consequences leading to the onset of autism. Studies have demonstrated that decreased I_f current might affect Shank3 haploinsufficiency, a protein which is located in synapses and is associated with disorders of the autism spectrum [39].

The association between HCN channels and schizophrenia has been attributed to the interaction mode of cAMP with HCN channels, which is necessary for modulating the likelihood of channel opening. An imbalance in this interaction has been associated with the risks of causing a disconnection from the signaling network at the prefrontal cortex (PFC), the area which is responsible for the execution of the working memory, learning, reasoning and understanding, and leading to the onset of schizophrenia [40]. However, a readjustment of the cAMP level in the cell makes it possible to reduce these effects [41].

The association between HCN malfunction and mood disorders has been highlighted in the studies on the effect of these channels on modulating anxiety and depression.

In the animal models of the depression disease, it has been shown that mice with the suppressed TRIP8b gene demonstrated a motor learning deficit as well as resistance to animal sinking into despair. Similar behaviors were also observed in mice whose genes HCN1 and HCN2 were missing. Additionally, treatment with ZD7288, an inhibitor of HCN channels can cause effects similar to antidepressants such as fluoxetine [42,43]. Furthermore, it has been shown that inhibition of I_f current in certain areas of the brain would be beneficial on the level of stress, anxiety and fear in an individual [44].

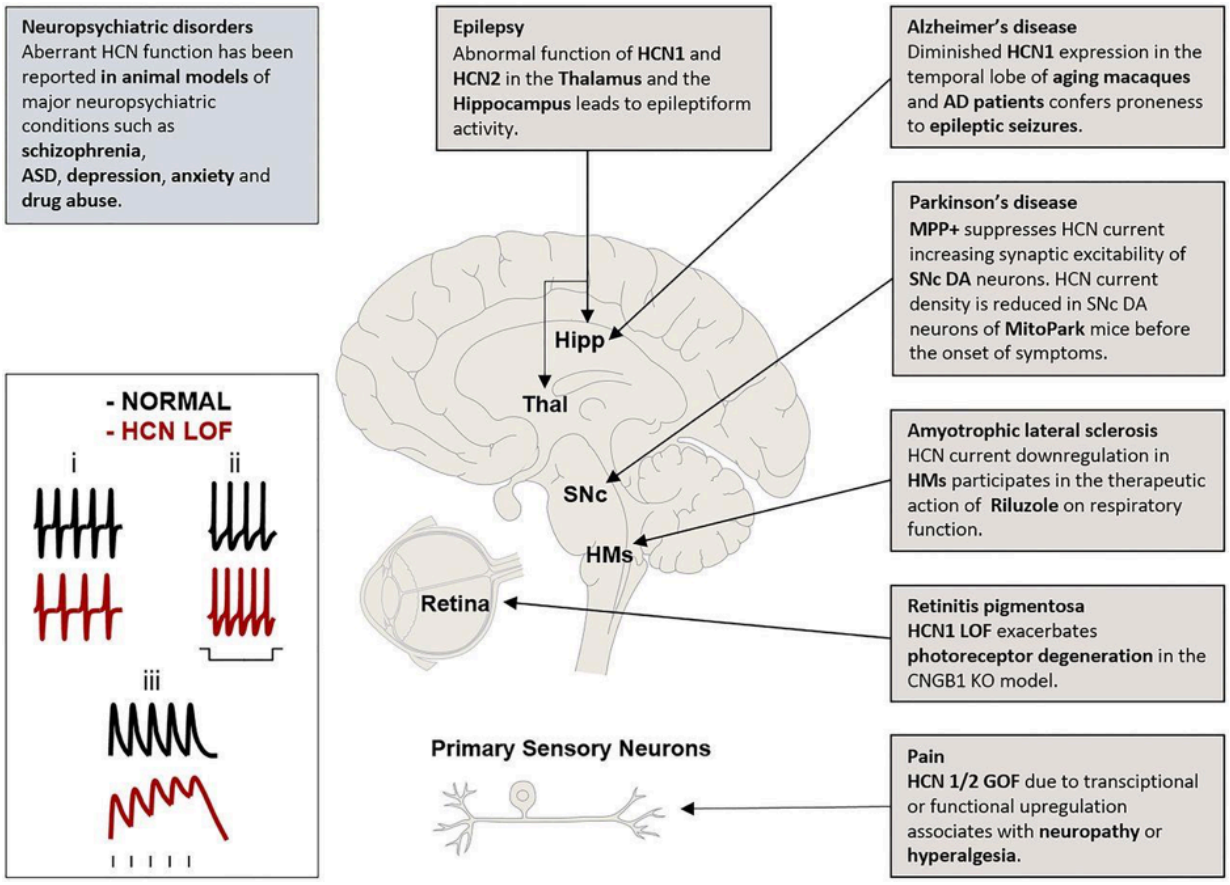

Figure 3. Implications of pathologies of dysfunction of HCN channels in CNS and PNS listed by preclinical and clinical studies [33].

1.2- Sequence and structure of HCN channels

1.2.1- Family of HCN channels

HCN channels belong to the voltage-gated ion channel superfamily (Fig. 4) [33]. Considering the number of members, it is ranked the third largest signaling protein superfamily, following the G protein-coupled receptors and the protein kinases. The members of the family have probably evolved from an ancestral protein with two transmembrane (TM) helices such as the bacterial KcsA channel. These 2TM channels have been further patched with an auxiliary 4TM transmembrane domain for voltage-dependent gating. Appendage of further intracellular or extracellular domains with the capacity to induce allosteric conformational shifts upon binding to different small molecules have produced extraordinarily versatile signaling molecules with

capacity to respond to voltage signals as well as those coming from intracellular/extracellular effectors and to integrate information coming from these two distinct types of inputs [4].

YU ET AL.

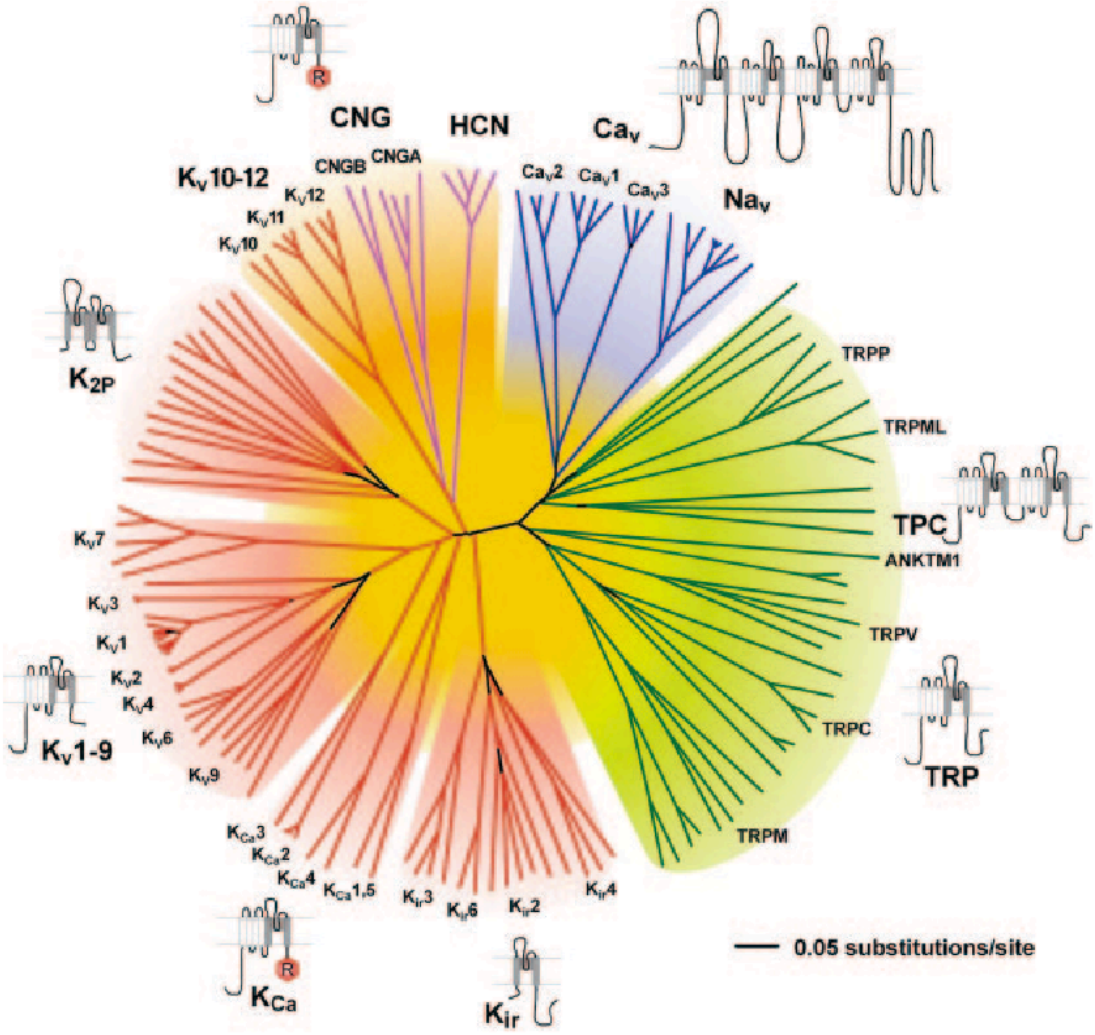

Figure 4. Representation of the amino acid relationships of the minimal pore regions of the voltage-gated ion channel superfamily [4].

The sequence of these channels has been molded into three functional zones: ion conductance, pore gating, and regulation zones. The ion-conducting pore and selectivity filter are formed by TM5 (S5) and TM6 (S6) segments and the membrane re-entrant pore loop (P-loop) between them [4,45-51]. Within 2TM potassium channels such as KcsA, the M1 and M2 segments are analogous to TM5 and TM6 and represent the ion conductance and pore gating zones. These segments are arranged in an upside-down teepee-like structure within the closed stated of the channel. In this

inverted cone-like conformation, the extracellular mouth of the cone is constricted by the intervening membrane re-entrant pore loop. This structure is cradled by the M1 and M2 transmembrane segments. A cavity in the center of the structure is water-filled and contains permeating potassium ions. The ion permeation path is blocked at the intracellular end by crossing of the M2 helices [52]. The addition of the TM1 to TM4 (S1 to S4) segments to the pore structure in the Nav, Cav, and Kv channels packs these channels with voltage sensor domain and confers voltage-dependent pore opening. This zone and mainly S4 segments, have repeated motifs of positively charged amino acid residues which undergo major translocations upon their fluctuations in membrane electric field. This motion in turn leads to S6 helices falling apart at the intracellular end and opening the channel gate [53,54]. In addition, the auxiliary ligand binding domains could exert a torque on the S6 segments that opens the pore by bending this helix upon ligand binding and facilitate the channel opening [55,56].

1.2.2- Sequence arrangement of HCN1 channel

Human genome holds four genes that encode HCN channel isoform (HCN1, 2, 3, 4) each yielding a protein of almost 770-1200 amino acid long [15,16]. The sequential arrangement of these residues give rise to each of the four monomers of the HCN channel, which is composed of the following subdomains; an intracellular N-terminal domain (also known as HCN domain) packed against five consecutive transmembrane (TM) helices (voltage sensor domain) followed by a pore-forming domain which is composed of TM5 (S5) helix, the small pore helix oriented oblique to the pore axis, and a re-entrant loop (selectivity filter) plus the 6th transmembrane helix. Two accessory domains are hanging from the end of the TM6 (S6) helix at the intracellular side of the channel; the C-linker domain and the cyclic nucleotide binding domain (CNBD) (Fig. 5). The transmembrane channel core consists of six alpha-helical segments (S1–S6) and an ion conducting pore loop between S5 and S6 [57].

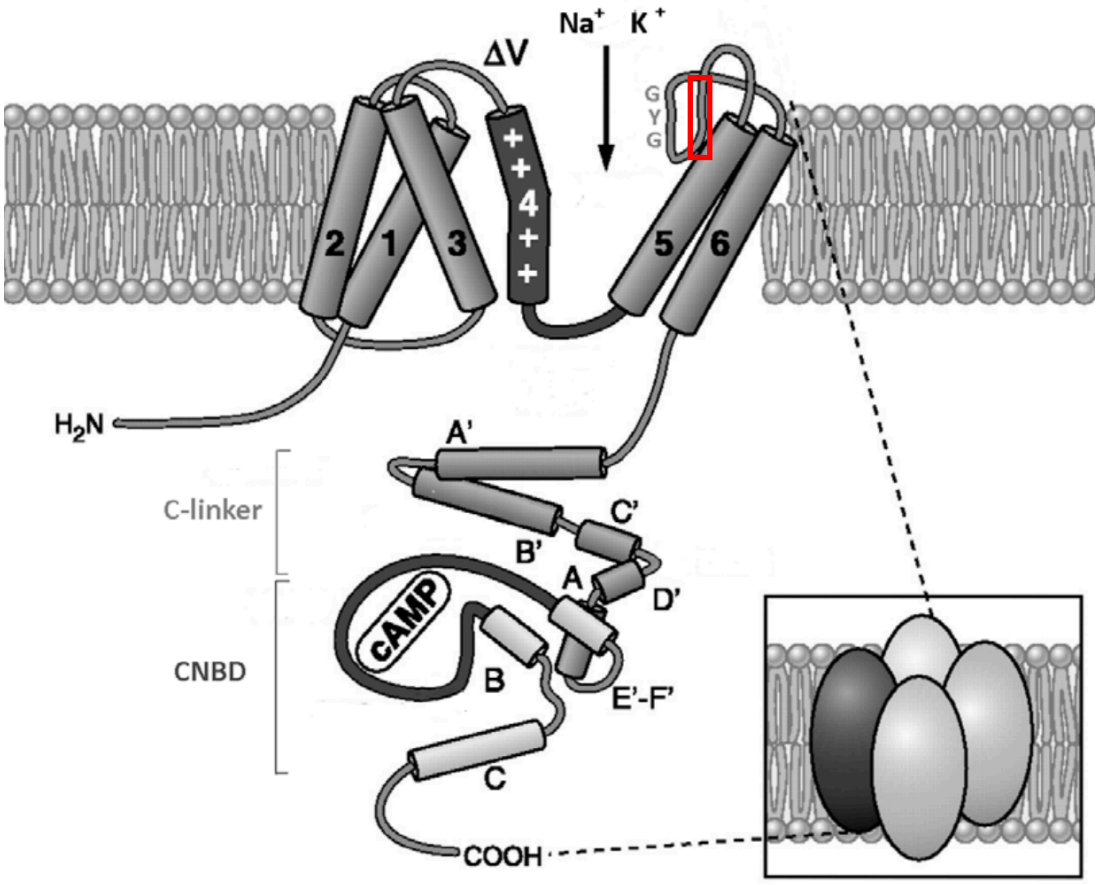

Figure 5. The topology of the HCN channel subunit [57]. The pore helix is highlighted by the red box behind the selectivity filter.

1.2.3- Structural architecture of HCN channels

The attempts to resolve the total structure of HCN channels have led to the determination of several cryo-EM structures representing the open and closed states of the HCN1 channel [5,6]. According to these structural data, the overall architecture of HCN channel is highly resembling that of the Kv channels [5,6]; The channel is composed of four identical subunits which are assembled in the membrane to form a 4-fold symmetric pore made by helices S5 through S6 (Fig. 5). This pore is surrounded by membrane-embedded voltage sensors (helices S1 through S4), similar to Kv channels (Fig. 6A). However, HCN channels have several subtle structural differences which allows them to fulfill their unique and eccentric role; the S4 segment of HCNs is relatively longer compared to Kv channels and is responsible for the unique voltage dependent opening of HCNs gate at hyperpolarization voltages of membrane. Additionally, the voltage sensor domain (helices

S1 to S4) in HCN1 are "non-swapped" contrary to the domain swapped conformation of Kv channels. It means each voltage sensor of each monomer contacts the pore through amino acids from the same subunit. However, in case of Kv channels such as Kv1–Kv9 and voltage-dependent Na^{+} and Ca^{++} channels, the channel assumes the domain swapped conformation in which the residues of voltage sensors from one subunit interact with the pore region of the adjacent subunit (Fig. 6 B) . At the C-terminal end, the S6 helices make a sharp bend and give rise to a helix-turn-helix "C-linker," also known as α-helical disk, just below the membrane. The C-linker is followed by chain five additional short α helices (C′- to F′- and A-helices) and a β-jelly roll that gives rise to the cyclic nucleotide binding domains (CNBDs) (Fig. 6A and C). Four CNBDs—one from each subunit—are docked onto the cytoplasmic face of the C-linker disk from the same and neighboring subunit (Fig. 6 A and C). The HCN channel exhibits an additional unique structural feature; The 45 amino acids preceding S1 give rise to a 3-α-helical domain that is wedged between the voltage sensor of the same subunit and the cytoplasmic domains of the neighboring one (Fig. 6A). This domain is unique to HCN channels, and therefore, has been known as the HCN domain [5,6].

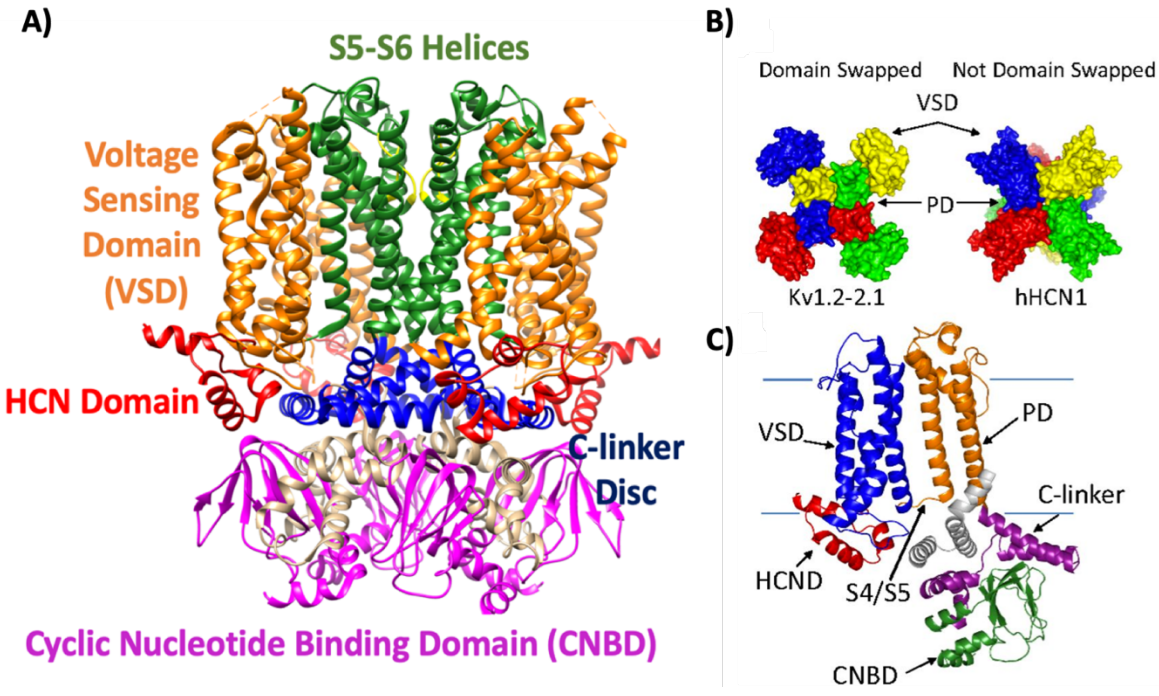

Figure 6. Structure of HCN1 channel. **A)** The structure of HCN1 channel tetramer in the ligand-free and closed state, viewed from parallel to the membrane. **B)** The interaction of different subunits of the channel in the domain swapped conformation of Kv1.2-2.1 channel and in the non-domain swapped conformation of HCN1 channel [58]. **C)** the topological arrangement of different domains in each monomer of HCN1 [58].

1.3- Selectivity filter in HCN channels

1.3.1- Ion selectivity and permeation in HCN channels

HCN channels are weakly selective for K^+ over Na^+ ions with a permeability ratio (PK/PNa) of 3–5 and are also considerably less permeable to Ca^{++}. However, they are the only know channels to select between Na^+ and Li^+ ions, making HCN channels semi-selective channels, rather than non-selective like the closely related CNG channels [15,16,59,60].

The ion selectivity of HCN channels is matched to their physiological roles. In fact, HCN channels are activated by hyperpolarized states and are constitutively active at rest [61]. Additionally, these channels allow for slow and semi-selective permeation of Na^+ and K^+ ions along their electrochemical gradient [15,62]. these features allow for modulation of membrane excitability by stabilizing the membrane potential against both excitatory and inhibitory inputs. For example, in some neurons as well as the sinusoidal cells of the heart, HCN channels regulate action potential firing and membrane excitability via the hyperpolarization-activated current I_h (also called h-current or funny current or I_f). To produce this current, HCN channel leaks Na^+ and K^+ ions at the resting potential of the cell (around −60 mV). HCN channels also have relatively a high permeability to Na^+ ions compared to K^+ channels [15,62]. This leads to gradual increase in membrane potential and triggering a rhythmic and spontaneous action potential [63]. It may also worth noting that the single channel conductance of HCN channels is less than 2 pS when measured in very high concentrations of potassium [64,65]; which is much smaller than the corresponding values of 5–50 pS that have been determined for potassium channels measured at physiological potassium concentrations [66].

1.3.2- Comparing the selectivity in HCN and Kv channels

The sequence of selectivity filter residues in HCN channels is highly conserved and highly resembling that of selective voltage dependent potassium channels (Kv). However, unlike the Kv channels, HCNs are not highly selective and allow the passage of sodium ions (Na^+) vs potassium (K^+) in a1:4 ratio. In addition, the HCN channels are not blocked by bromide ions (Br^+) or tetraethylammonium (TEA) [15]. Comparing the selectivity filter sequence between HCN channel and those of selective Kv channels suggest for the overall conservation of the sequence. However,

there are subtle differences in the selectivity filter. As shown in figure 7, K^+ channels have a pore-lining sequence of T(V/I)GYG. By contrast, HCN channels have a pore-lining sequence of CIGYG. Interestingly, the cysteine substitution for threonine in an attempt to restore the conserved TIGYG sequence in Kv channels, fail to restore the compromised selectivity pattern in HCN channel compared to Kv channels [60,67]. Therefore, it seems that the observed radical differences in selectivity pattern between HCN and Kv channels would be due to other factors such as the difference between the network of interactions between selectivity filter residues and those of the pore helix which precede the selectivity filter (Fig. 5 and Fig. 7). These interactions have already been proved to have a determinant role in regulating the mechanism of selectivity in Kv channels [68,69]. In fact, it has been shown that the conserved network on hydrogen bond interactions between the sidechain of pore helix residues and those of the selectivity filter reinforces the proper spatial alignment of pore residues in Kv channels and could contribute to the proper orientation of selectivity filter carbonyl groups toward the pore interior [68,69]. As shown in figure 7, The conserved tryptophan in Kv channels (Kv1.1, Kv1.4 and KcsA) is substituted by Phenylalanine in HCN channels. This could lead to perturbation of the aforementioned hydrogen bond network and interfere with the ability of the pore filter K^+ from Na^+ ions.

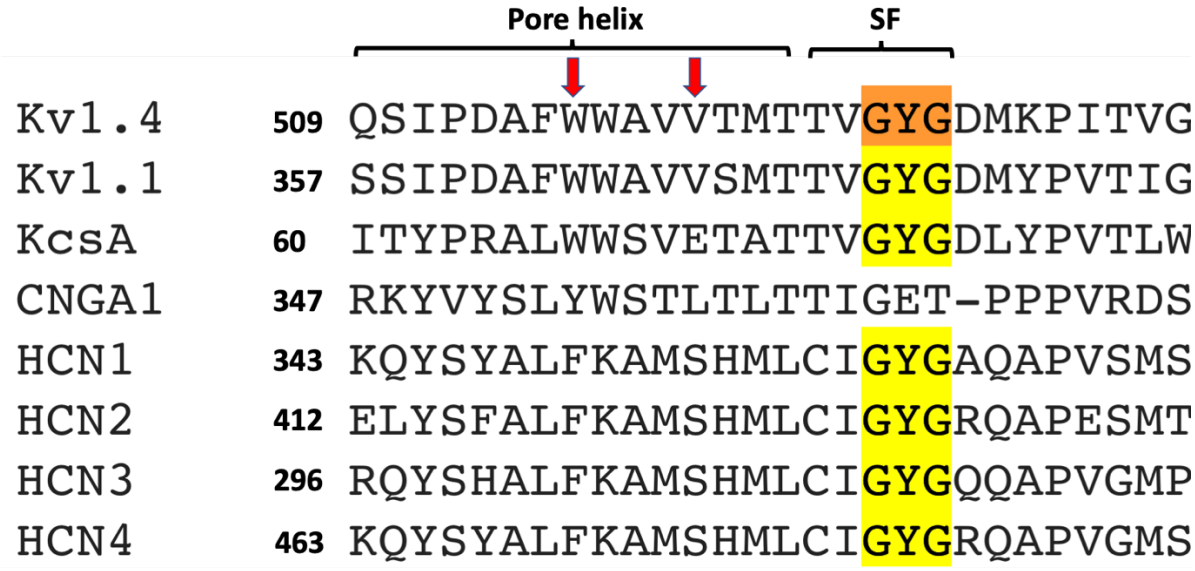

Figure 7. Amino acid sequence of selectivity filter and pore helix in HCN, CNG and KV channels. The sequences of the selectivity filter and pore helix are highlighted. SF: selectivity filter.

Such subtle differences in the sequence arrangement of selectivity filter and pore helix residues could affect the orientation of selectivity filter in HCN channel compared to Kv channels. As shown in figure 8, in case of Kv channels, the backbone carbonyl groups of selectivity filter residues are arranged in a cylindrical shape and give rise to four equally spaced ion-binding sites known as S1-S4 sites from top to bottom [52,70]. In this symmetrical arrangement, each ion sits in the middle of a cubic cage and at each site, a K^+ ion is coordinated by eight oxygen atoms from carbonyl groups of the selectivity filter (Fig. 8). This tight and synchronous coordination of K^+ ions has been accounted responsible for sieving these ions from smaller Na^+ ions which interact asynchronously [52].

However, the selectivity filter residues of HCN channel are oriented in a funnel shape structure with S1 and S2 sites eliminated due to wide open funnel mouth and disorientation of carbonyl groups (Fig. 8) [5]. Additionally, the conserved threonine residue which gives rise to S4 in Kv channels site is substituted with cysteine in HCN channels (Cys358 in HCN1) [5]. According to the structural clues based on the cryo-EM structure of HCN1 channel, the binding site is more dilated compared to Kv channels and the ion can bounce up and down between the S3 and S4 sites [5]. Therefore, the permeability of HCNs, among other things, could stem from the greater distance between the propellers of this filter. These observations may justify the 20–fold lower selectivity for K^+ over Na^+ ions in HCN channels compared to K^+ channels [15,71,72].

To explain the mechanism of ion permeation in K^+ channels, two main mechanisms have been proposed based on the results of biochemical and structural studies; several studies have supported a soft knock-on mechanism in which water molecules are co-transported along with K^+ ions, while other studies have supported a hard knock-on mechanism in which only K^+ ions are found in the selectivity filter [73]. However, the soft knock-on mechanism has been mainly accepted as the mechanism for K^+ ion permeation along the selective K^+ channels. According to this model, the five S0 to S4 ion binding sites, are occupied by 2-3 K^+ ions interspersed by water molecules and hence through the net translocation of each K^+ ion through the membrane, one water molecule is translocated as well [74]. However, analysis of ions dynamics in simulations of bacterial Na^+ channels shows that despite the prevalent mode of alternating occupancy of the channel by 2-3 ions, the aforementioned knock-on mechanism is loosely coupled to the permeation mechanism [75-77]. Additionally, as the narrowest part of the pore is significantly wider than that of K^+ channels, ions remain at least partly hydrated while permeating through the Na^+ channel.

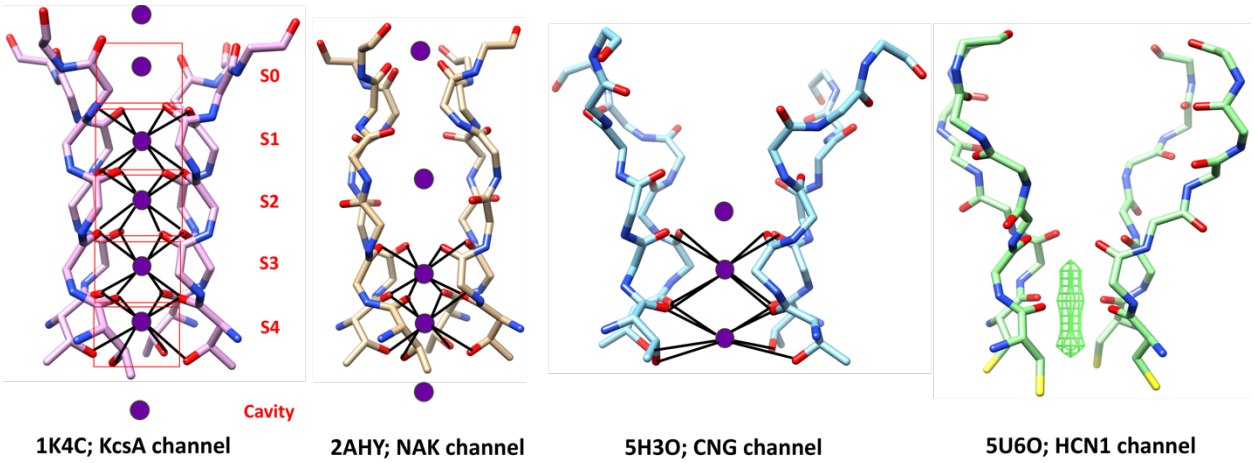

Figure 8. The structural arrangement of selectivity filter residues in HCN channel versus CNG, NaK and KcsA channels. The red boxes represent the conventional S0 to S4 sites for binding the K+ ion in Kv channels.

1.3.3- Comparing the selectivity in HCN and CNG channels

Based on structural similarities, cyclic nucleotide-gated (CNG) and HCN channels are close relatives among the members of the superfamily of voltage-gated cation channels (Fig. 9) [4,78]. Despite the overall structural similarity, the two channel classes differ from each other with regard to their mode of activation. CNG channels gating process is independent of membrane voltage and these channels are opened by direct binding of cAMP or cGMP. However, HCN channels are mainly regulated by voltage fluctuations and fully open upon membrane hyperpolarized and close upon depolarization. Despite this, cAMP can directly bind to HCN channels at the intracellular site and increase the channel opening probability by shifting the voltage dependence of channel activation to more positive membrane potentials and thereby facilitating voltage-dependent channel activation [16,59,79].

Similar to CNG channels, HCN channels also seem to have two binding sites at S3 and S4 sites. However, CNG and HCN channels reveal distinctive ion selectivity patterns. Although both channels pass monovalent cations such as Na^+ and K^+, CNGs do not discriminate between them. Additionally, Ca^{++} permeation rate is much higher CNG channels compared to HCNs [80,81].

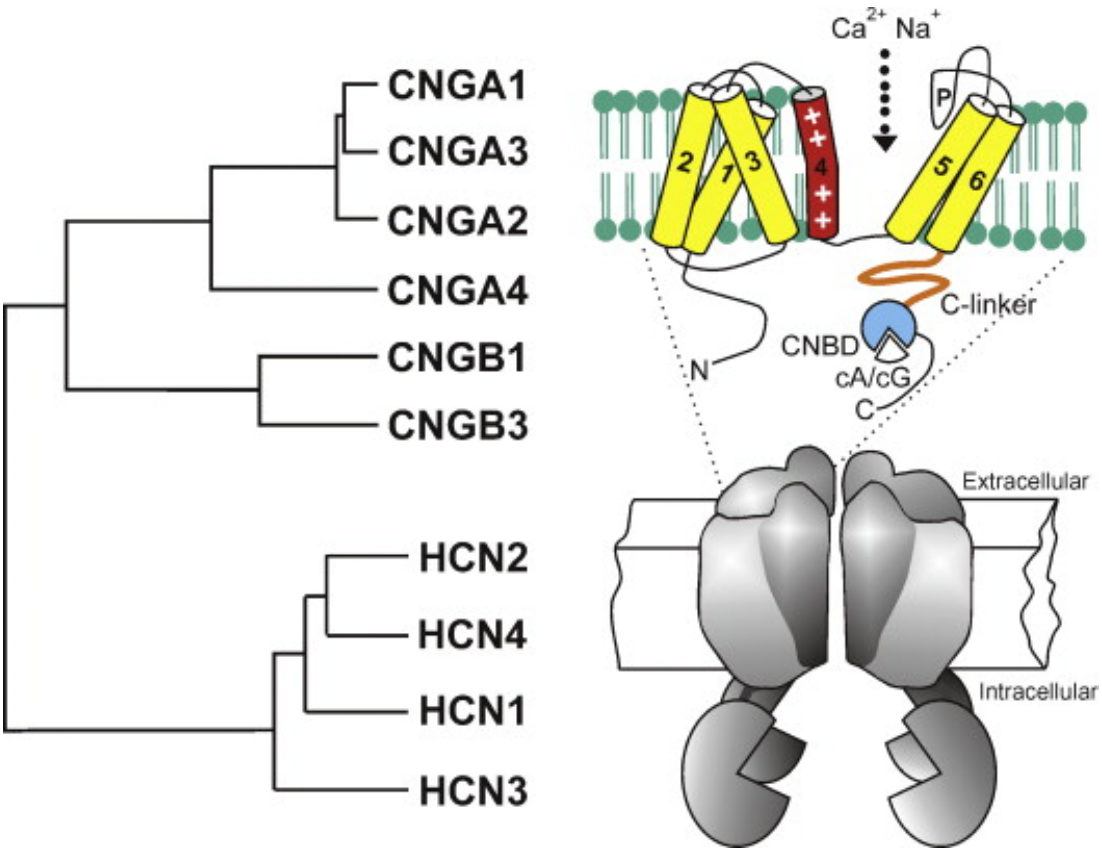

Figure 9. Phylogenetic tree and structural model of cyclic nucleotide-regulated cation channels [78].

The pore of CNG has three bonding sites formed by a combination of acidic residues sidechains and backbone carbonyl oxygens. According to the cryo-EM structure of the CNG channel, the diameter of the selectivity filter ranges between 4.7-10.1 Å in this channel [82]. However, the pore seems to be tighter in HCN and with a diameter of around 5 Å [5]. The dilatated selectivity filter in CNG channels allows for ion with one or more hydration water to pass through feature has been attributed to the low selectivity of the CNG channels. Additionally, unlike the delicate hydrogen-bonding network surrounding the selectivity filter of K^+ channels, the selectivity filter of CNG channel is mainly reinforced by hydrophobic interactions. This may provide more flexibility for the selectivity filter residues to properly arrange around different cations and may not force the CNG channel to sieve the ions based on their sizes [82].

The number of binding sites is also an important factor in determining the mechanism of the selectivity; it has been shown that in channels that favor K^+ binding over Na^+, multi-K^+ ion

occupancy will increase the probability that a Na^+ will exit from the same side it entered (because there is a K^+ ion blocking the other side due to its higher affinity) and thus permit kinetic selectivity. this phenomenon that has already been demonstrated in the NaK channel [83-85].

2- MD simulation for studying ion channels

2.1- From electrophysiology to MD simulations

Ion channels carry charges across the membrane. Because of this, their diffusion rate can be measured using electrical recording techniques of electrophysiology. Such experiments typically provide the first glimpse on how ion channels work. Using voltage clamp experiments on a giant squid axon in 1950s, Hodgkin and Huxley were able to identify the first ever voltage-gated cation K^+ and Na^+ currents and deduced how these channels contribute to the propagation of the action potential [86]. However, understanding the structure-function relationship of the ion channels is highly crucial to understanding their involvement in a wide range of fundamental physiological functions and therapeutic applications. In this regard, the use of MD simulations greatly contributed to the current understanding on the molecular basis of ion selectivity and ion permeation [75,87].

The basis for conventional view on ion selectivity was a rigid pore that is solely optimized for coordinating K^+ ions and not for Na^+ ions [88]. However, in reality proteins have a rather fluid-like, dynamic structure with rapid conformational fluctuations [89]. Hence, the ion-protein interactions and their association with ion permeation should be studied in a dynamics context and not be limited to a single structure. Molecular dynamics (MD) simulation is a reliable approach which is are capable of generating an ensemble of conformations corresponding to a conducting channel modeled based the initial crystal structure. These conformations are generated based on formulating physical principles which accounts for the experimentally-observed properties of biomolecules [90]. Therefore, MD simulations can provide a temporal view of the mechanism of ion conductance and selectivity at atomic-level resolution.

2.2- Molecular dynamics simulation to study voltage gated ion channels

Modeling and simulations of ion channels are generally limited by the experimental knowledge about them. Predicting the structure of a membrane channel from its sequence is considered a formidable task for studying ion channels at atomistic resolutions and the "no structure, no study" rule is generally adopted by the majority of researchers working in the field. Among the different computational approaches for studying ion channels, all-atom molecular dynamics (MD), Brownian dynamics (BD), and approaches based on Poisson−Nernst−Planck (PNP) theory, are the most prevalent ones. The MD method is considered the most computationally expensive but also the most accurate [91].

Prior to the availability of experimentally determined 3D structure of HCN channels covering the whole protein sequence, several MD simulation studies have been performed to determine the nature of cAMP binding to CNBD domains and deciphering the atomistic details of such interaction on channel gating [92-94]. Additionally, a homology modeling approach to reconstruct the HCN structure in closed and open states and based on the structure of KcsA and Calcium-gated potassium channel MthK, provided some insight on the overall arrangement of amino-acid residues in these two functional states [95]. A state of art MD simulation study on the mechanism of gating and the role of S4 helix in this regard has shown how S4 helix sharply bends during the gating process and splits into two sub helices which in turn induces an splaying motion in S5 helix which provides the space for S6 helices to move apart and open up the pore [96].

2.2- Rational for studying ion selectivity in HCN channel by MD simulation

To the best of our knowledge, no experimental or computational studies has been performed to elucidate the atomistic interactions that could explain the mechanism of selectivity in HCN channels. Despite the availability of several cryo-EM structures on the whole sequence of HCN1 channel, the precise localization of the ions in the selectivity filter is not clear in any of them [5,6]. This could be due to the fact that ion is not to be stably localized in the S3 or S4 site, judged by the green mesh representing the plausible location of K^+ ion in cryo-EM structure [5,6]. Additionally, the density map of water molecule is very similar to that of K^+ ion and make it hard to confidently decide on precise ion localization in the static structure derived from cryo-EM approach. Besides, the static picture provided by cryo-EM is not able to clearly reflect the dynamics behavior of the selectivity filter and in the presence of near-native environment.

The importance of studying the dynamics of selectivity filter to understand the mechanism of selectivity and the underlying atomistic interactions has been reflected in several studies on Kv and CNG channels [68,97,98]. For example, in case of CNG channels, a close relative of HCNs, MD simulations indicates that the side chain of Glu66 in the selectivity filter can assume multiple conformations and the diameter of the pore changes significantly along the simulation, depending on the nature of cation present in the selectivity filter [97]. The crystal structure often reflects the conformation trapped in the global minimum of free energy landscape and such conformations that visit different local minima are barely captured in crystallographic and cryo-EM studies. However, accessing a dynamic perspective of channel structure, and selectivity filter in this case, seems to be indispensable to understand the mechanism of selectivity. Such knowledge could be gained through the application of MD simulation.

It should be noted that depending on the size of the system being studied in terms of the atom numbers, all-atom MD simulations could be very computationally expensive and at the same time, the reliability of the results could be highly affected by time-window of the simulation being performed. In fact, several phenomena such as channel gating would demand milli-seconds to seconds of simulation while ion conductance or main-chain/side-chain motions of amino acids could be captured in nano- to micro-second time scales [99]. In this study we performed the simulations on 200 ns time scale which seems to be sufficient for finding the stable binding mode of the ions in the selectivity filter.

3- The idea of Molecular dynamics simulation

3.1- Calculating atoms trajectory based on potential energy function

The main idea of MD simulation is to calculate and implement the equations of the motion of atoms from the potential energy function:

Based on this notion, in a system composed of N interacting particles, the force acting on each particle, i, is estimated by the gradient of the potential energy with respect to atomic displacement (equation 1.1);

$$\vec{F_i} = -\nabla_i U \qquad (1.1)$$

Following the calculation of forces, Newton's law of motion, $\vec{F} = m\vec{a}$ (equation 1.2), can be used to numerically solve the motion of the particle i;

$$\overrightarrow{F_i} = m_i\overrightarrow{a_i} = m\frac{d\overrightarrow{v_i}}{dt} = m\frac{d^2\overrightarrow{r_i}}{dt^2} \quad (1.2)$$

In the above equation, m, a_i and v_i represent mass, acceleration and velocity, respectively, of the i^{th} particle at time t. The variable $\vec{r_i}$ represents the position vector of particle i in a cartesian coordinate system.

The following equation (equation 1.3) provides the value of $\vec{r}$ at time t + δt as a function of acceleration ($\vec{a}$), initial position ($\vec{r_i}$) and the initial velocity ($\vec{v_i}$) at time t. Here, δt refers to the time step of the simulation, which typically falls within the range of few femtoseconds (fs) in order to ensure that the change in forces over one timestep is small and the fasted motions are accounted for;

$$\vec{r_i}(t + \delta t) = \vec{r_i}(t) + \vec{v_i}(t)\delta t + \frac{\vec{a_i}(t)\delta t^2}{2} \quad (1.3)$$

Once the new position of each particle, $\vec{r}$ (t + δt), is computed, the process is iterated; the interatomic forces are updated in order to calculate the subsequent positions after another time step. This entire process is repeated to obtain a trajectory of coordinates of the system for a finite time period. A number of numerical algorithms have been developed for integrating the equations of motion. In this study, the Leap-frog algorithm is employed [100].

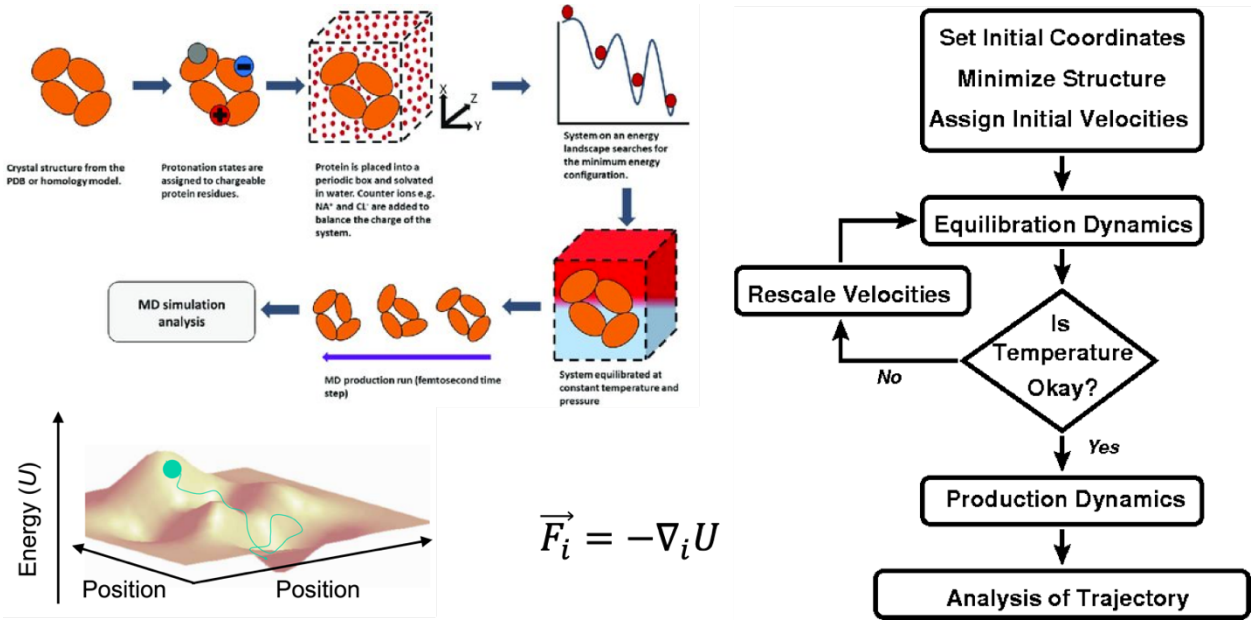

Figure 10. A schematic representation of the molecular dynamics processes.

3.2- Temperature and pressure control

In the context of classical statistical mechanics, temperature is treated as a direct measure of the average molecular kinetic energy and the definition of the temperature in a (classical) many-body system makes use of the equipartition theorem, which conceptually means that at thermal equilibrium, each independent degree of freedom has an equal amount of kinetic energy; for example, the average kinetic energy per degree of freedom in the translational motion of a molecule is equal to its rotational motions. Thus, according to the equipartition theorem, the average kinetic energy, ⟨K⟩, per degree of freedom is related to the thermodynamic temperature, T, in the following way (equation 1.4);

$$\langle K \rangle = \frac{1}{N}\sum_{i=1}^{N}\frac{1}{2}m_i v_i = \frac{1}{2}k_B T \quad (1.4)$$

where m_i, v_i, and k_B represent the mass, velocity of the particle, i, and Boltzmann constant, respectively. In practice, the measure of the total kinetic energy normalized by the number of unrestrained degrees of freedom, N_f , is used to compute the instantaneous temperature, T_i (equation 1.5):

$$T(t) = \sum_{i=1}^{N}\frac{m_i {v^2}_i(t)}{k_B N_f} \quad (1.5)$$

Here, $v_i(t)$ refers to the velocity of particle, i at time (t). In order to conduct simulations under constant temperature or constant pressure, various temperature and pressure coupling algorithms are employed. For example, a temperature coupling algorithm may involve velocity rescaling at each time step or stochastic impulsive forces that act occasionally on randomly selected particles. All approaches of pressure coupling algorithm involve the scaling of the volume of the simulation box. In this thesis, Nosé–Hoover algorithm [101] and the Parrinello-Rahman algorithm [102] were employed for temperature- and pressure- coupling, respectively.

3.3- Periodic boundary conditions

Biomolecular simulations usually involve bulk systems, such as a solid crystal or protein in a solution. In MD simulations, a system containing the desired molecules is prepared in a finite simulation box due to limited computer memory and also to speed up all the calculations. By translating copies of the simulation box in 3D space, periodic boundary conditions allow the simulation of a bulk system and eliminate edge effects in a finite simulation box.

3.4- Water molecules

Ignoring the solvent (the molecules surrounding the molecule of interest) leads to major artifacts. There are two main options for taking solvent into account; Explicitly represent solvent molecules or the Implicit solvent modeling. The latter option is less accurate despite being faster and is a mathematical model to approximately represent the average effects of solvent.

The explicit models are determined based on the parameters derived from quantum mechanics, molecular mechanics and experimental results. The models of water molecules could be classified into different categories based on; (i) the number of interaction points called site, (ii) whether the model is rigid or flexible, (iii) whether the model includes polarization effects or not. In this study we used the TIP3P water model which is a three-point rigid water molecule with charges and Lennard-Jones parameters assigned to each of the 3 atoms of the molecule [103].

3.5- MD simulation package and forcefield

In order to compute atomic trajectories by solving equations of motion numerically, empirical force fields have been developed. In other words, a force field is a mathematical expression describing the dependence of the energy of a system on the coordinates of its particles. In this context, molecules are simply defined as a set of atoms that are held together by simple elastic (harmonic) forces and the force field replaces the true potential with a simplified model valid in the nano-environment being simulated. The parameters of the energy functions may be derived from experiments in physics or chemistry, calculations in quantum mechanics, or both (and hence the name empirical force fields). All-atom force fields account for the parameters for every type of atom in the system, including hydrogen. However, united-atom interatomic potentials provide a cruder representation (for higher computing efficiency) and treat the hydrogen and carbon atoms in each methyl group (terminal methyl) and each methylene bridge as one interaction center.

In recent years, many popular simulation packages, such as Amber, Gromacs, and NAMD, have all embraced the parallel computing as well as powerful GPUs based computing using CUDA library [104]. In the current study, we used NAMD software package to perform the MD simulation [105]. NAMD enables the use of few force fields such as AMBER [106], CHARMM [107], and OPLS [108],

but not GROMOS96 [109]. Here, we used the CHARMM all-atom forcefield which is widely used for simulating the protein-membrane systems.

4- The manuscript on the structural dynamics of selectivity filter in HCN channel

ION BEHAVIOUR IN THE HCN1 CHANNEL SELECTIVITY FILTER

Sajjad Ahrari and Nazzareno D'Avanzo

From the Département de phramacologie et physiologie, Université de Montréal, Montreal, Canada, H3T 1J4

Address for correspondence: Ph: (514) 343-5634, FAX: (514) 343-7146,
e-mail: nazzareno.d.avanzo@umontreal.ca

Keywords: **HCN1, Ion channel, MD simulations, ion selectivity,**

ABSTRACT

Hyperpolarization-activated cyclic nucleotide-gated (HCN) channels are responsible for the generation of I_h in cardiac and neuronal cells. Despite the overall structural similarity to voltage-gated potassium (Kv) channels, HCNs show much lower selectivity for K^+ over Na^+ ions. This increased permeability to Na^+ is a critical to its role in membrane depolarization. HCNs are also one of the only known proteins to select between Na^+ and Li^+ ions. Here we investigate the unique selectivity properties of HCNs using molecular dynamics simulations. Our simulations suggest that the HCN1 pore is flexible and dilated compared to Kv channels with only one stable ion binding site within the selectivity filter. We also observe that ion co-ordination and hydration differ within the HCN1 selectivity filter compared to Kv and CNG channels. Additionally, the C358T mutation further stabilizes the symmetry of the S4 site and provides a more fit space for ion coordination, particularly for Li^+.

Introduction

Hyperpolarization-activated cyclic nucleotide-gated (HCN) channels belong to the voltage-gated cation channel superfamily. The 4 HCN isoforms (HCN1-4) are responsible for the generation of I_h in cardiac and neuronal cells where they play a role in setting the resting membrane potential, pacemaking, dendritic integration, , and establishing action potential threshold[1]. HCN channels are important for learning and memory[2,3], pain sensation[4], sour taste sensation[5], and vision[6]. Ivabradine is an approved drug for the symptomatic management of stable heart-related chest pain and heart failure[7] and there are strong efforts in recent years to screen for novel I_h inhibitors for the treatment of epilepsy, pain, schizophrenia, addiction and other neurological disorders [8,9].

HCN channels are composed of four subunits consisting of six transmembrane alpha helices, and a C-terminal cyclic-nucleotide binding domain (CNBD) that is attached to the S6 transmembrane domains via an 80 amino acid linker[10]. The S1-S4 transmembrane domains of each subunit generates a non-domain swapped voltage-sensor domain (VSD), which is arranged next to the pore-forming S5-S6 helices of the same subunit. Recent atomic resolution structures have also identified a novel N-terminal domain HCN-domain[11,12], which couples cyclic-nucleotide binding to voltage-gating[13]. Despite the overall structural similarity to voltage-gated potassium (Kv) channels, HCN channels demonstrate 20-fold lower selectivity for K^+ over Na^+ ions (P_{Na}/P_K = 0.2-0.3 in HCNs [14], compared to Kv channels [15]. This increased permeability to Na^+ ions results in a net influx of Na^+ ions, and is a critical to the role of HCNs in depolarizing cellular membranes. Intriguingly, HCNs are one of the only known proteins that can select between Na^+ and Li^+ ions, making HCN channels semi-selective, rather than non-selective like the closely related CNG channels. Differences in selectivity between selective channels like Kv channels, and non-selective channels such as CNGs, have been partially attributed to multi-ion vs single-ion binding in the selectivity filter [16]. In non-selective channels, the selectivity filter residues orient differently than selective Kv channels, rendering the top of the pore wide-open, eliminating the first (and possibly second) ion binding sites [17] (Fig. 1A). In addition to the 3D arrangement of pore-forming residues, the dynamic behavior of the selectivity filter in the presence of various cations could have a major effect on ion selectivity. Structures of HCN1 indicate a wide-open top of its selectivity filter, similar to CNG channels. However, it remains unknown how many ions stably bind within the HCN pore, and what enables HCN channels to maintain semi-selectivity. Here, we investigate the

unique selectivity properties of HCN channels using molecular dynamics (MD) simulations. Our simulations suggest that the HCN1 pore is dilated with a very high degree of flexibility, with only one stable binding site for partially hydrated ions within the selectivity filter. Additionally, the co-ordination of K^+ ions with the carbonyl groups of the selectivity filter is more stable compared to Na^+ and Li^+ ions, which may explain the channel's distinct selectivity properties. We also investigate why the conversion of the HCN selectivity filter sequence (CIGYG) to that of selective Kv channels (TIGYG) (Fig. 1B) fails to restore the compromised K^+ selectivity in HCN channels[18,19].

RESULTS

Dynamics of ions' motions within the selectivity filter of WT HCN1

To identify the most stable binding sites for K^+, Na^+, and Li^+ ions in the HCN1 pore, we performed all-atom MD simulations. In separate simulations for each ion type, ions were placed in the S0, S1, S3, S4 and cavity (C). No ion could be placed in the S2 site because the carbonyl groups are flipped away from the conduction pathway, and the tyrosine sidechain makes the site becomes unavailable for ion binding. The ions were constrained for the first 20ns of production simulations, in order to enable the carbonyl groups of the pore to adjust their arrangement around each ion and ensure the ions did not leave the pore simply due to an unfavourable starting arrangement. The trajectory of ion movement within the selectivity filter over the course of the simulation time for each ion is presented in Fig. 2. After 20ns, all constraints were lifted, ions that were initially located at S1, S3 and S4 pop out of the pore and irreversibly join the solvent phase. The ion which was initially localized within the cavity migrates to the S4 site, remains partially hydrated, and is co-ordinated by the carbonyl groups of Cys358 and water molecules. Since no structure of the open HCN1 pore is available, our simulations were performed with the closed pore conformation, which prevents the cavity from being replenished with another ion. Therefore, to evaluate whether the ion that moves from the cavity into the S4 site gets trapped there because there is no additional ion to repel it over the energy barrier into the S3 site, (through either a hard or soft knock-on mechanism), we performed an additional set of simulations for each ion type (Fig. S2). In these simulations, only one ion (either K^+, Na^+ or Li^+) was placed in the selectivity filter at the S3 site. The placement of the ion at S3 position also provides further insight on the ability of this site to coordinate the ion and serve as a stable ion binding site. In these systems, shortly after initiating the simulations, the ion migrates from the S3 to the S4 site (Fig S2), with the ion coordinated by the carbonyl backbone of C358 and waters, similarly to the other set of simulations (Fig. 2). Again, this is ion behavior was consistent for K^+, Na^+, and Li^+ ions. This indicates that regardless of how the simulations are performed, the S4 site is the only stable binding site within the selectivity filter of HCN channels.

A careful examination of ion movement within the selectivity filter indicates that ions fluctuate along the Z axis between the plane of C358 carbonyl groups and lower into the S4 site as ions are coordinated in other K^+ channels (Fig. 2). The ions frequently sample the plane of the C358 carbonyl groups (black lines), a feature that appears unique to HCN channels. Additionally,

ions are partially hydrated with only two of the four selectivity filter subunits participate in coordinating the ion (Fig. 3). This differs from observations in Kv and CNG channels [16,20,21] where ions are either dehydrated in the selectivity filter (in Kv channels) or synchronously coordinated by carbonyl groups from all 4 subunits (in both CNG and Kv channels). This is made evident by measuring the distance between the ion and the carbonyl groups of C358 from each subunit. For K^+ and Na^+ ions, the distance between the ion and C358 carbonyl groups of subunit C and D are 2.8 Å and 2.5 Å respectively, while the distance of these ions to the C358 carbonyl groups of subunit A and B are greater than 5 Å (Fig. 3A and 3B). We observe similar results for Li^+ ions when we examine various snapshots during the trajectory, however, Li^+ ions move more freely in the x-y plane than K^+ and Na^+ ions, therefore the distribution of distances to are more diffuse (Fig. 3C). However, a peak at 2.2 Å is observed, which indicates that Li^+ ions also regularly closely approach the C358 carbonyl groups. In fact, RMSD measurements for the ions stably sitting in S4 of the pore follow the same selectivity sequences measured electrophysiologically[18] with K^+ showing the most stable behavior in the pore, followed by Na^+ and then Li^+ (Fig. S1).

Taken together, these results suggest that there is only one primary binding site in HCN1 selectivity filter located. This site is at the S4 position, formed between the carbonyl oxygen of C358 and the sulfhydryl group of its sidechain. The off-center location of ions in the pore, high mobility of these ions between HCN subunits, and overall lack of a second stable binding site in the pore may all contribute to the low (~1pS) conductance observed for HCN channels [22].

Hydrated ion coordination within WT HCN1 selectivity filter

It is evident that ions permeating through potassium selective pores do so mostly dehydrated [20,21]. However, our simulations indicate that cations permeating through HCN channels are partially hydrated. We examined the number of water molecules coordinating each ion at the S4 position throughout the trajectory using ion-oxygen cut-off distances of 3.6 Å for K^+, 3.2 Å for Na^+ and 2.8 Å for Li^+[23]. Our analysis indicates that each ion spends the majority of the time coordinated by four water molecules in addition to the 2 carbonyl groups of the C358 residue (Fig. 3, right panel). In case of K^+ and Na^+, two of these waters are arranged to fill the gap between the ion and the carbonyl groups from the opposing non-coordinating subunits. The other two water molecules interact with the ions such that they do not interfere with direct interaction between ion and the carbonyl groups (Fig. 2). This arrangement of coordinating water molecules and carbonyl

groups stabilize the off-center localization of K^+ and Na^+ ions. In case of the Li^+, the ion is more tightly coordinated by four water molecules, which generally prohibits direct interaction between Li^+ and the C358 carbonyl groups. As a result, the Li^+ ion sits slightly lower than the C358 carbonyl plane compared to K^+ and Na^+. It should be noted that during the simulation time the sulfur atoms of Cys358 sit very far apart and at around 7 to 9 Å distance (Fig. S2). In this regard, the S4 site resembles a small cavity which has merged with the bottom cavity and cannot assume a caged-like structure to accommodate the ion. Therefore, while partially hydrated K^+ and Na^+ ions move along the z-axis between the carbonyl plane of C358 and into the wide S4 site while remaining partially coordinated with the carbonyl oxygens, the Li^+ ion becomes fully hydrated rapidly, and primarily wanders in this wide opening of the S4 site.

Limited hydrogen bond network behind the HCN1 selectivity filter helps to stabilize S4

Ion binding, permeation, conductance and selectivity in potassium channels are all partially determined by the rigidity of the selectivity filter [24,25] [26]. A hydrogen bond network between residues on the pore-helix and the selectivity filter residues in potassium channels help to keep the carbonyl groups facing the conduction pathway and forming multiple ion binding sites. As a result of this hydrogen bond network behind the pore, the distance of the carbonyl groups remains narrow enough to favour the coordination of dehydrated ions in the center of cage-like binding sites formed by the eight carbonyl groups of the selectivity filter residues (Fig. 1). Our MD simulations indicate that in HCN1 channels, this hydrogen bond network is limited to the lower part of the selectivity filter (Fig. 4B and Table S1), with hydrogen bond interactions stabilizing the pore facing orientation of C358 and to a lower extent I359. Specifically, the C358 residue is stabilized in this orientation through hydrogen bonds formed with H355 via their backbone. This C358-H355 hydrogen bond is uniformly present in all 4 subunits in all the simulated systems (Table 1). Additional hydrogen bonds are formed between G360-S354 and I359-S345, however, these hydrogen bonds are not uniformly observed between HCN1 subunits.

In addition, the protonated imidazole side chain of H355 also forms a stable electrostatic interaction with D312 (Fig. 4A). This interaction appears to further stabilize the H355 backbone orientation to enable formation of the C358-H355 hydrogen bond (Fig. 4A). Intriguingly, the propensity to form the H355-D312 salt-bridge again follows the pattern of ion selectivity (Fig. 4A), with this salt-bridge formed more frequently in the trajectory of simulations with K^+, than

Na^+, and least frequently for Li^+. This suggest that while the selectivity filter may stabilize ion binding at S4 in the HCN1 pore, the ions also contribute to the stabilization of the HCN1 selectivity filter.

Ion dynamics and coordination within the selectivity filter of HCN1 C358T

The role of the pore-lining Cys residue in HCN permeation and selectivity has been examined previously by electrophysiological experiments[18,19]. Mutations of the CIGYG selectivity filter sequence in HCN channels to the typical TIGYG selectivity filter sequence of Kv channels fails to confer K^+ selectivity to HCN channels[18,19]. In fact, the equivalent C358T mutations increases ion conductance by ~30%, increases the permeation of Na^+ and Li^+ ions, enables the permeation of large quaternary ammonium ions such as TMA, and abolishes the channels' ability to select between Na^+ and Li^+ ions[18]. To understand why C358T does not favour K^+ selectivity, but rather enables improved passage of Na^+ and Li^+ ions, we performed additional sets of MD simulations on HCN1 C358T channels. Similar to what we observed in simulations of the wild-type channel, after 20ns when all constraints on the ions were removed, ions that were initially located at S1, S3 and S4 moved rapidly out of the pore and irreversibly join the solvent phase (Fig. S5). The ion which was initially localized within the cavity migrates to the S4 site, remains partially hydrated. However, in C358T the ions are notably localized below the carbonyl groups of Thr358, rather than in same plane. Moreover, especially in the case of Li^+, the ion appears more stable this lower position on the z-axis, as the ions in the S4 site less frequently move to the plane of the T358 carbonyl group compared to ions in the wild-type system. This behavior of Li^+ is also reflected in the variations of the RMSD plot which is indicative of a much narrower structural fluctuation in the mutated system bearing the Li^+ ion (Fig. S1). We also observe that in simulations of C358T, the K^+ ions move towards the central pore axis, as evident by the more uniform distribution of distances between K^+ and the carbonyl oxygen groups (~2.8 Å for all 4 subunits), the increase in number of coordinating carbonyl groups, and the reduced number of coordinating waters (Fig. S6). To a lesser degree we see a similar effect with Na^+ ions (Fig. S6), however, the higher degree of hydration still prevents the Na^+ ion from fully approaching the central pore axis. This shift towards the central axis, and lower position of the ion in the S4 site, may contribute to the small (~30%) increase in ion conductance observed in HCN2 and HCN4 channels with the

equivalent C358T mutations[18,19], since the strength of the ion-carbonyl interaction would be reduced and an incoming ion would be more likely to knock the ion through.

The effect of C358T on the geometry and dynamics of the HCN1 selectivity filter

Similar to the wild-type systems, the selectivity filters of both wild-type and C358T HCN1 channels are wide enough to accommodate partially hydrated Na^+ and the fully hydrated Li^+ ions. However, by examining the distribution of distance between the oxygen atoms of the T358 sidechain, we see that the pore diameter varies from 4.2 Å to 9.2 Å (depending on the ion) (Fig. S2). This is narrower and more stable compared to corresponding distance between the sulfur atoms of the C358 in wild-type HCN, which varies between 5.2 to 10.2 Å (depending on the ion) (Fig. S2). In the case of K^+ ions, the narrower carbonyl groups and sidechain oxygen atoms of T358 now enable the dehydrated ion to be directly coordinated by 4 carbonyl groups and 4 side-chain hydroxyl groups with water molecules now forced to engage directly above and below the K^+ ion (Fig. S5), similarly to Kv channels, (Fig. S5 and Fig. S6). While C358T pore at this position also narrows compared to WT HCN1 channels in the presence of Na^+ and Li^+ ions, their hydration shell prevents as tight a restriction as that observed for K^+. In this regard, it seems that the C358T mutation tightens the S4 site and provides a more uniform space for ion coordination (Fig. S5 and Fig. S6). These results provide further evidence for a highly dynamic pore in HCN channels.

Measurement of the flipping motions for the carbonyl groups of the SF shows a similar pattern to that of the wild-type system (Fig. S7), with only the T358 carbonyl group constantly facing the pore-axis, while the remaining selectivity filter residues rapidly rearrange their orientations. Additionally, a similar pattern of hydrogen bonding is observed between the backbone atoms of the SF and the residues behind the pore (Table S1). Similar to wild-type system, the hydrogen bond between the backbone of T358 and H355 residues has the highest consistency among the different HCN1 subunits and as a result the pore would have a more synchronous behavior at the T355 site. Intriguingly, we observed the sidechain of T358 is also stabilized by a persistent hydrogen bond to the backbone of the neighboring L357 residue (Table S1 and Fig. S8). This stable hydrogen bonding seems to be very important to fix the side-chain of T358 towards the pore axis and enable the coordination of dehydrated K^+ and partially or fully hydrated Na^+ and Li^+ ions deeper into the S4 site (Fig. S8). Lastly, the electrostatic interactions between the side-chains of D312 and H355 persist in these sets of simulations as well.

DISCUSSION

Potassium channels have the backbone carbonyl groups of selectivity filter residues arranged in a cylindrical shape, gives rise to four equally spaced ion-binding sites known as S1-S4 sites from top to bottom [20,21]. In this symmetrical arrangement, a K^+ ion in is coordinated by eight oxygen atoms from carbonyl groups of the selectivity filter as if sitting in the middle of a cubic cage. This synchronous coordination of K^+ ions in-turn helps the carbonyl groups remain oriented toward the conduction pathway and enables multiple K^+ ions to be coordinated in the pore, allowing for rapid ion conductance via a "hard" or "soft" electrostatic repulsion (knock-on) (Fig. 5A). According to our results, the selectivity filter in HCN1 channel is more dynamic than a Kv pore, with only one binding site (between carbonyl groups of C358) stably present during the simulation time. Additionally, the dilated pore with a diameter of around 5 Å accommodates the partially hydrated K^+ and Na^+ ions as well as the fully hydrated Li^+ ion either in plane with the C358 carbonyl groups or slightly deeper into the S4 binding site. However, unlike what is observed for potassium and CNG channels [16,20], in HCN channels, ions do not reside along the central pore-axis, but rather partially hydrated ions are co-ordinated in an offset manner more reminiscent of what is observed in Nav and Cav channels. We propose that the high mobility of a partially hydrated ion within the pore, and number of and distance to the co-ordinating carbonyl groups that we observe in our studies, and the highly flexible and destabilized outer pore region (which reduces the frequency of observing stable S1, S2, and S3 binding sites), all contribute to the low (~1 pS) conductance of HCN channels. Therefore, it is conceivable that the formation of an outer site may occur infrequently, and when it does, ions may permeate in either direction by electrostatic repulsion (ie. soft or hard knock-on) (Fig. 5B). However, since this outer site is rarely stable, the equilibrium highly favours a single-ion occupied pore. This model is supported by our simulations where an ion was placed in the S3 site, and it readily moved back into the S4 site.

Our data does enable us to provide some insights on ion selectivity in HCN channels, however, given the time-course of our simulations, and the closed conformation of the pore (preventing us from fully observing conduction events), we are somewhat limited. Conventional views on the mechanism of selectivity in ion channels proposed a "snug fit" model in which accounts for the rigidity of the filter and fitting the ion in the pore according to its Pauling radius [27]. This model assumes the ion to be stripped off from its water shell and this dehydration energy being compensated by synchronous coordination of ion by selectivity filter oxygen atoms. Recent

insights however propose a dynamic model in which the selectivity filter has liquid-like properties and selectivity is yielded as a result of several factor such as the effect of strain energy (which accounts for structural perturbation of the host (e.g. selectivity filter) as the result of guest (e.g. ion) presence in the context of host–guest chemistry), chaperone-like effect of the ions (which accounts for the necessity of ions presence to avoid SF collapse), in addition to ion hydration-dehydration energy compensation[28-30].

Potassium channels have a 100-1000 fold higher selectivity for K^+ over Na^+ and Li^+ ions [31]. It has been argued that the multi-ion arrangement in the potassium channel pore contributes to both rapid ion conduction and a high degree of ion selectivity. Studies using NaK channels [32-34] suggest that multi-K^+-ion occupancy increases the probability that a Na^+ will exit from the same side it entered (because a K^+ ion would be blocking the other side due to its higher affinity) and thus permit kinetic selectivity. Additionally, smaller ions such as Na^+ and Li^+, have different dehydration energies which may exclude them from the entering the pore (a molecular sieve). However, even once they can be dehydrated enough to enter the pore, Na^+ ions interact asynchronously with the selectivity filter carbonyl backbones and contribute to rapid rearrangement of the carbonyl backbone away from the conduction path (flipping), and in some cases pinching or collapse of the conduction pathway [28].

On the other end of the spectrum are CNG channels, which are effectively non-selective between monovalent cations. Recent atomic structures indicate that the lack of the external tyrosine and glycine residues in their selectivity filter sequence of CNG channels results in the elimination of the outer (S1) ion binding site[16]. The three remaining potential ion binding sites are again formed by a combination of backbone carbonyl oxygens and hydroxyl oxygen of the threonine residue sidechains, and a continuous elongated density can be observed across all three sites in the atomic resolution structure. This suggests multi-ion binding within the CNG pore, despite their inability to effectively discriminate between K^+, Na^+ and Li^+ ions [16,35]. In fact, MD simulations using the engineered NaK2CNG-E channels suggest that the dilated selectivity filter in non-selective CNG-like channels may bind up to 2 partially hydrated ions with the inner (or lower) ion residing largely in the S3 site along the central pore axis. However, unlike the delicate hydrogen-bonding network surrounding the selectivity filter of K^+ channels [24], the selectivity filter of CNG channel is mainly reinforced by hydrophobic interactions[16]. This results in a pore diameter of the CNG selectivity filter ranges between 4.7-10.1 Å[16] compared to the typical pore diameter of

1.7-5.4 Å in potassium channels [36]. This may provide more flexibility for the selectivity filter residues to properly arrange around different cations and may not force the CNG channel to sieve the ions based on their sizes[16].

It is clear from our studies here that ion selectivity cannot arise simply from presence or absence of multi-ion binding within the pore, or by the pore acting purely as a molecular sieve, since HCN channels can still select between K^+, Na^+, and Li^+ ions[18,19,37]. It is also evident that the sulfhydryl group of C358 does not act like the rate-limiting barrier as previously proposed[18], since the atomic structure, and our MD simulations, do not indicate this sidechain to ever act as the narrowest restriction point in the pore. However, it was demonstrated previously that HCN selectivity is reduced when the pore lining cysteine is mutated to threonine (C358T equivalent) [18]. Considering our simulations of WT and C358T HCN1 channels, we provide the following insights into HCN selectivity. In the wild-type HCN, the K^+ and Na^+ ions in the selectivity filter are shielded by water molecules or CO groups of C358. In other words, the lower dehydration energy of the ion (compared to Li^+) allows for stripping several water molecules from the ion and its direct interaction with carbonyl groups of C358. Therefore, the ion is localized close to the carbonyl groups during the simulation. However, in case of Li^+ ion, the higher dehydration energy (compared to K^+ and Na^+ ions) barely allows for stripping the water molecules and the direct interaction of the ion with carbonyl groups. Accordingly, the shielded Li^+ ion is abandoned to wildly jiggle in the wide open S4 site. This behavior reduces the chance of synchronous coordination of ion by the selectivity filter, (which is demanded for attracting the ion to the binding site and its permeation to either site) and leads to lower chance of Li^+ ion permeation compared to K^+ and Na^+. Upon the C358T mutation, the Li^+ ion, which is still shielded by water molecules and sitting in the S4 site, experiences a tighter space due to being more tightly surrounded by Thr358 CO groups and its sidechains. This relatively tighter packaging of the shielded Li^+ ion at S4 site limits the jittering motions of the ion and increases the chance of its synchronous coordination by selectivity filter and hence its permeation. This observation could explain the higher permeation rate of Li^+ ion upon C358T mutation [67].

Interestingly, in the mutant structure and in case of K^+ ion, the S4 site assume a tight conformation and leaves no gap for the water molecules to sneak in and mediate the ion interaction with CO groups. In other words, the ion is stripped off from shielding water molecules (except for one water molecule at the top and one at the bottom of ion) and directly binds to CO groups of

T358. It seems that C358T mutation increases the chance of K^+ ion to act like a chaperone in gathering the oxygen atoms of T358 around itself and increasing the chance to delicate and precise coordination of the pore around this ion at the S4 site. Establishment of an ordered S4 site in the mutated structure seems to be highly dependent on the precise localization of the T358 sidechain which in turn depends on a stringent hydrogen bond between the sidechain of this residue and the backbone carbonyl group of L357 (Fig. S8).

The importance of the hydrogen bond network between pore residues and those of the pore helix in proper arrangement of selectivity filter CO groups has already been shown in several studies [24-26]. Interesting, L478T/C479T as well as S475E/C479T mutations in HCN4 channel (equivalent to L357T/C358T and S354E/C358T mutations in HCN1, respectively) failed to produce measurable current despite high levels of N-glycosylated protein expression[18]. As shown in Figure S9, these mutations seem to interfere with the network of hydrogen bond behind the pore and specifically those that keep T358 and I350 CO groups in place. In case of L357T/C358T mutations, the sidechain of T357 could be localized in a proper location to establish a hydrogen bond with the CO group of S354. This interaction could perturb S354 proper localization which in turn has an important role in reinforcing the hydrogen bond network behind the pore. Upon S354E mutation, the sidechain of E354 could rest at the very close vicinity of I359 NH group and by dragging the backbone of this residue toward itself could interfere with proper arrangement of T358 carbonyl group around K^+ ion. These effects would lead to disorientation of the CO groups at the only binding site of the pore and hence lead to compromised ion permeation along the pore.

MATERIALS AND METHODS

System preparation

Atomic models of HCN1 were constructed based on the Cryo-EM crystal structure of the protein (PDB ID: 5U6O[17]) in a closed conformation with a tightly packed inner helical bundle that constricts the pore to a radius of about 1 Å. Since HCN1 retains hyperpolarization-activated gating in the truncated form which is devoid of the C-linker and cyclic nucleotide binding domains (HCN1ΔCNBD)[42], these domains were omitted from the structure of HCN1 used in our simulations to reduce the system size and speed up simulation times. Therefore, the target model covered residues 94-402 (Uniport ID: O60741). To determine the favourable binding sites of K^+, Na^+ and Li^+ ions in the selectivity filter, 3 models for each system were built; In each model, four homogenous ions were placed at S1, S3, S4 and the cavity beneath the selectivity filter (Fig. 2). Both ions located at S1 and the cavity site were fully hydrated while the ions at S3 and S4 were directly exposed to carbonyl groups of the selectivity filter residue. For some simulations, a single K^+, Na^+ and Li^+ ion was placed in the S3 site of the selectivity filter and systems were rebuilt. For a 3rd set of simulations, a C358T mutation was introduced using Chimera UCSF software[43] and the systems were rebuilt for each ion condition. For each modeled structure, the pKa value of each reside was calculated with the PROPKA server[44], and all residues were assigned their standard protonation state at pH 7 accordingly. Consequently, His355, located on the pore helix, was protonated in our simulations, despite not being protonated in the cryo-EM structure which was resolved at pH 8[17]. The protein was then oriented appropriately for molecular dynamics simulations using the Orientation of Proteins in Membranes (OPM) webserver[45].

Molecular dynamics simulations

To prepare the microenvironment of the simulation, the channel was embedded in a bilayer of POPC lipids in all simulated systems and solvated in 150 mM of KCl (in case of K^+/Li^+ systems) or NaCl (in case of Na^+ systems) using the CHARMM-GUI web server[46]. The total number of atoms in the MD systems is on the order of 170000 atoms. The CHARMM36 force field[47] for protein, lipids, and ions was used. Explicit water was described with the TIP3P model[48]. Parameters for K^+ and Na^+ ions inside the channel were defined according to Roux and Berneche[49] and parameters for Li^+ ions were defined according to Lamoureux and Roux[23].

The prepared systems were refined using energy minimization for at least 2000 steps, and the ions and non-filter backbone atoms were kept fixed throughout the minimization procedure. After energy minimisation, the ions location in the conductive filter was restrained for 20 ns to relax any unfavourable contacts destabilising the selectivity filter. All the simulations were performed under constant NPT conditions at 310 K and 1 atmosphere, and periodic boundary conditions with electrostatic interactions were treated by the particle-mesh Ewald (PME) algorithm[50] with grid spacing less than 1 Å. A 12 Å smoothed cut off (10–12 Å) with switching distance cut-off of 10 Å was applied for the switching function to take effect for van der Waals interactions. The pressure was maintained at 1 atm using a Nose-Hoover Langevin piston control[51], with a period of 50 fs and oscillation decay time of 25 fs. To maintain the temperature, the system was coupled to the Langevin thermostat with damping coefficient of 1 ps^{-1}. Equations of motion were integrated at 2 fs time intervals. Bond lengths involving hydrogen atoms were constrained using the SHAKE algorithm as implemented in NAMD. The simulations were performed at time step of 2 fs. After minimization and equilibration with harmonic positional restraints on all of the C atoms, MD simulations were performed for 200 ns for wild type and all mutants, by using NAMD version 2.12, on the supercomputers of Compute Canada. Simulations were performed in two steps; an initial 20 ns restrained simulation with the ions' location in the selectivity filter constrained for 20 ns to relax any unfavourable contacts destabilising the selectivity filter. The harmonic constraint energy function was applied along all Cartesian directions with an exponent of 2 and scaling factor of 3. This initial phase was followed by 180 ns simulation with these constraints being lifted. All molecular graphics work and figures were provided using VMD[52] and UCSF chimera[43] software.

ACKNOWLEDGEMENTS

This work was supported by a National Science and Engineering Research Council (NSERC) Discovery Grant awarded to ND (RGPIN-2019-00373). SA was supported by scholarships awarded from the Université de Montréal. This research was enabled in part by support provided by Calcul Quebec (www.calculquebec.ca) and Compute Canada (www.computecanada.ca). Molecular Dynamics Simulations were performed using allocations on MP2, Helios, Graham, and Cedar clusters.

COMPETING INTERESTS

The authors have no competing interests to declare.

Table 1. Hydrogen bond network between selectivity filter and pore helix												
H-bond Pair	**H-bond percentage in WT**											
	POT				**SOD**				**LIT**			
	A	**B**	**C**	**D**	**A**	**B**	**C**	**D**	**A**	**B**	**C**	**D**
S354-G360	-	63	-	77	-	55	-	59	24	62	40	31
S354-I359	53	20	21	-	48	22	50	45	29	-	36	39
H355-C358	27	35	30	25	33	27	34	22	31	32	28	26
K351-Y361	-	-	-	-	40	-	-	-	-	-	-	-
H-bond percentage in C358T												
S354-G360	28	-	165	42	-	51	-	32	-	52	65	29
S354-I359	57	-	-	20	52	32	118	29	80	-	61	33
H355-C358	26	-	28	33	27	25	34	31	31	21	33	20
T358-L357	78	72	76	76	73	68	43	76	62	76	77	73
K351-Y361	60	-	-	-	-	35	-	-	-	-	40	-

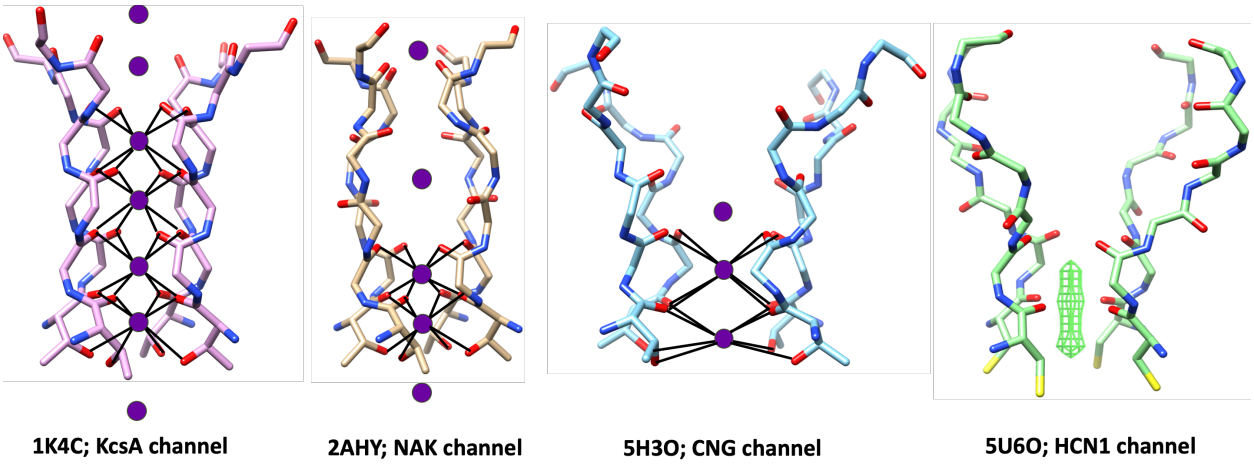

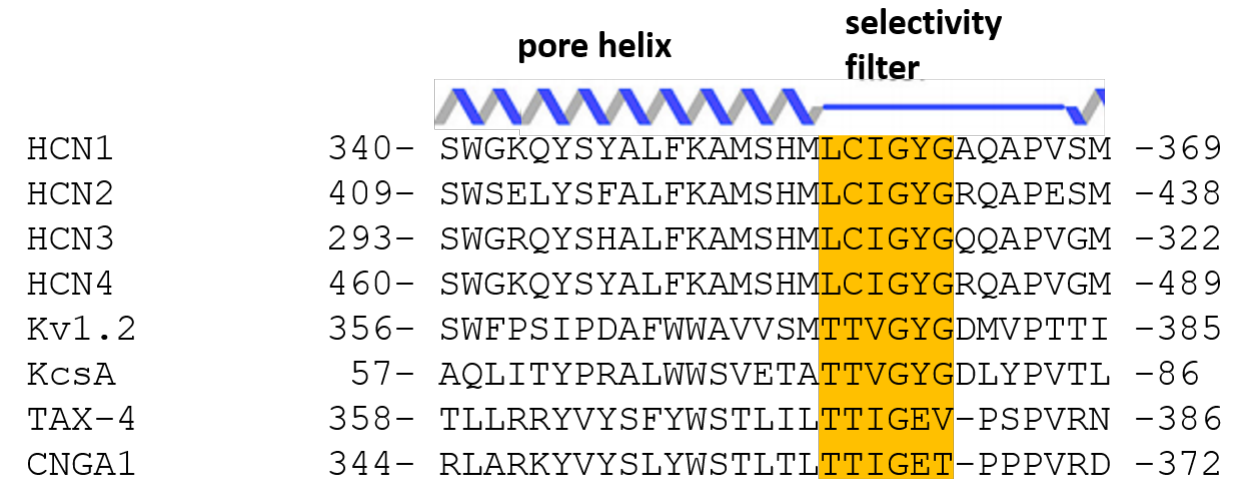

Figure 1. The arrangement of backbone atoms of the selectivity filter of KcsA, NAK, CNG and HCN channels. (*top*) The four letter codes represent the PDB ID of each protein. The number of ions in the selectivity filter are represented in spheres, with the black lines indicating the coordination by carbonyl and sidechain oxygens. (*bottom*) Sequence alignment of the pore-helix and selectivity filters (highlighted in orange) of HCNs, potassium and CNG channels.

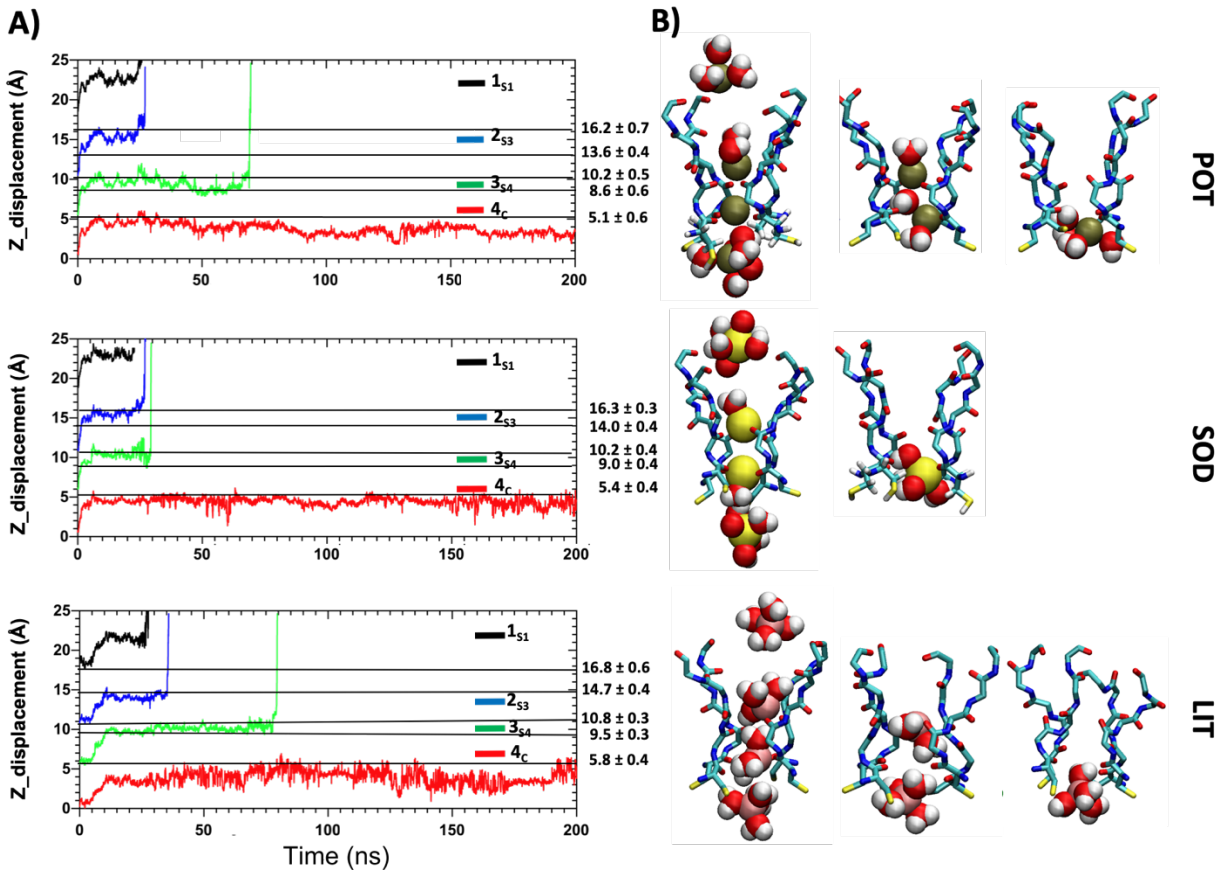

Figure 2. Identification of a single stable binding site for K^+ (POT), Na^+ (SOD) and Li^+ (LIT) ions in the HCN1 selectivity filter (A) Trajectory of K^+, Na^+ and Li^+ ions localization along the Z axis of selectivity filter over the time-course of the simulations. The geometrical localization of each ion within different zones of selectivity filter are highlighted by different colors. 1_{S1} (black) represents the ion number 1 which was initially positioned in S1 site. 2_{S3} (blue) represents the ion number 2 which was initially positioned in S3 site. 3_{S4} (green) represents the ion number 3 which was initially positioned in S4 site. 4_C (red) represents the ion number 4 which was initially positioned in bottom cavity site. The thin black lines in the background of each graph represents the average location carbonyl groups in the selectivity filter along the Z axis (from bottom to top: C358, I359, G360, Y361 and G362), with the specific values reported on the side of the graph. **(B)** Snapshots of the HCN1 selectivity filter with ions and their coordinating waters taken from the 20^{th} ns, 100^{th} ns and 200^{th} ns, respectively.

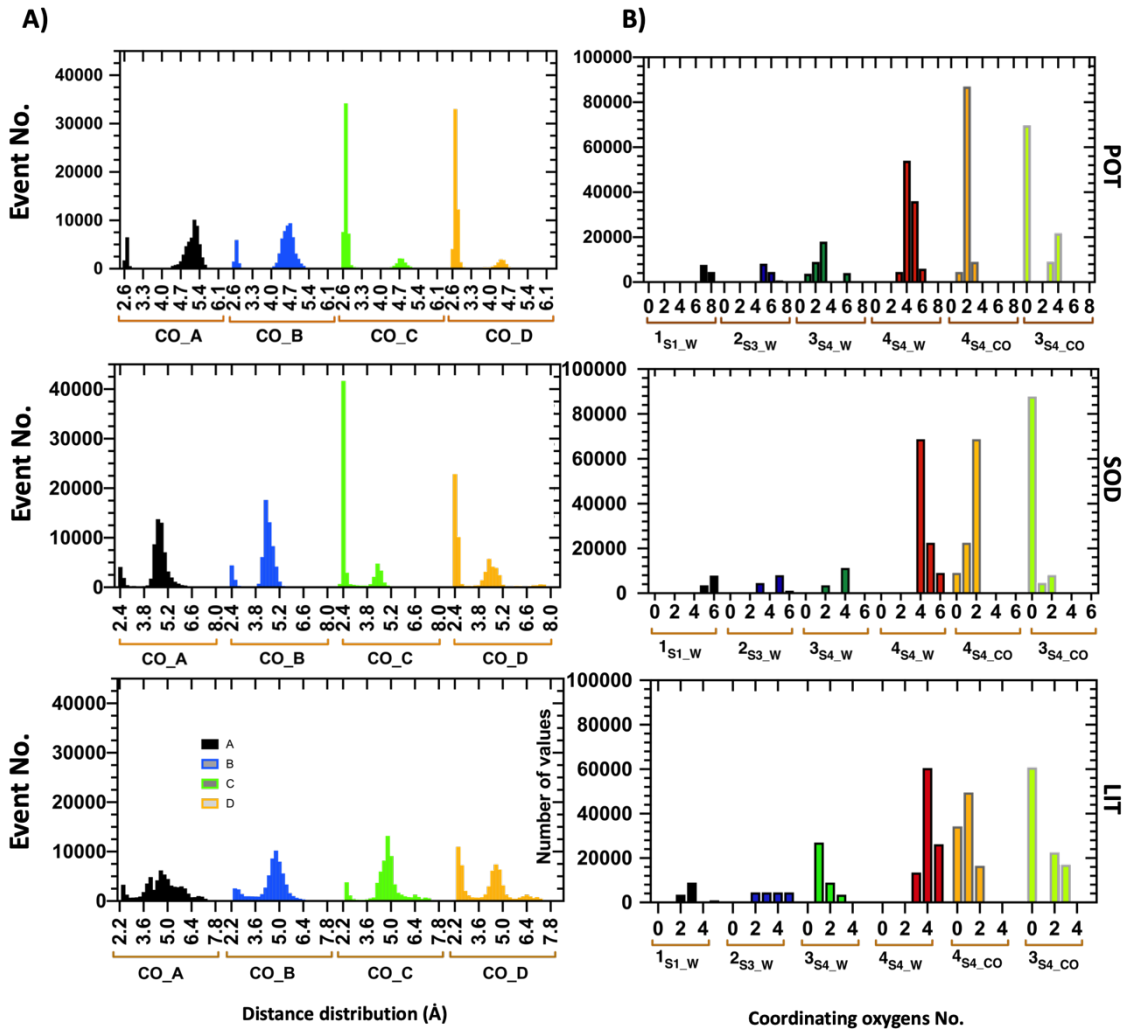

Figure 3. Ion coordination by C358 carbonyl oxygens and water. (A) Histogram for the distribution of distance (Å) between each ion and its coordinating oxygen atoms (from CO groups of C358). The caption under each graph represents the distribution of aforementioned distances for each protein chain. **(B)** Histogram for the number of oxygens (from water molecules or backbone of selectivity filter residues) that coordinate each ion during the simulation. The captions under each graph represent the ion number and its location in the selectivity filter; 1_{S1_W} represents water molecules that coordinate ion number 1 initially localized at S1 site. 2_{S3_W} represents water molecules that coordinate ion number 2 initially localized at S3 site. 3_{S4_W} represents water molecules that coordinate ion number 3 initially localized at S4 site. 4_{S4_W} represents water molecules that coordinate ion number 4 following its translocation to S4 site. 4_{S4_CO} represents carbonyl groups that coordinate ion number 4 following its translocation to S4 site. 3_{S4_CO} represents carbonyl groups that coordinate ion number 3 while localized at S4 site. The CO_A, CO_B, CO_C and CO_D represent the carbonyl groups from chain A, B, C and D, respectively.

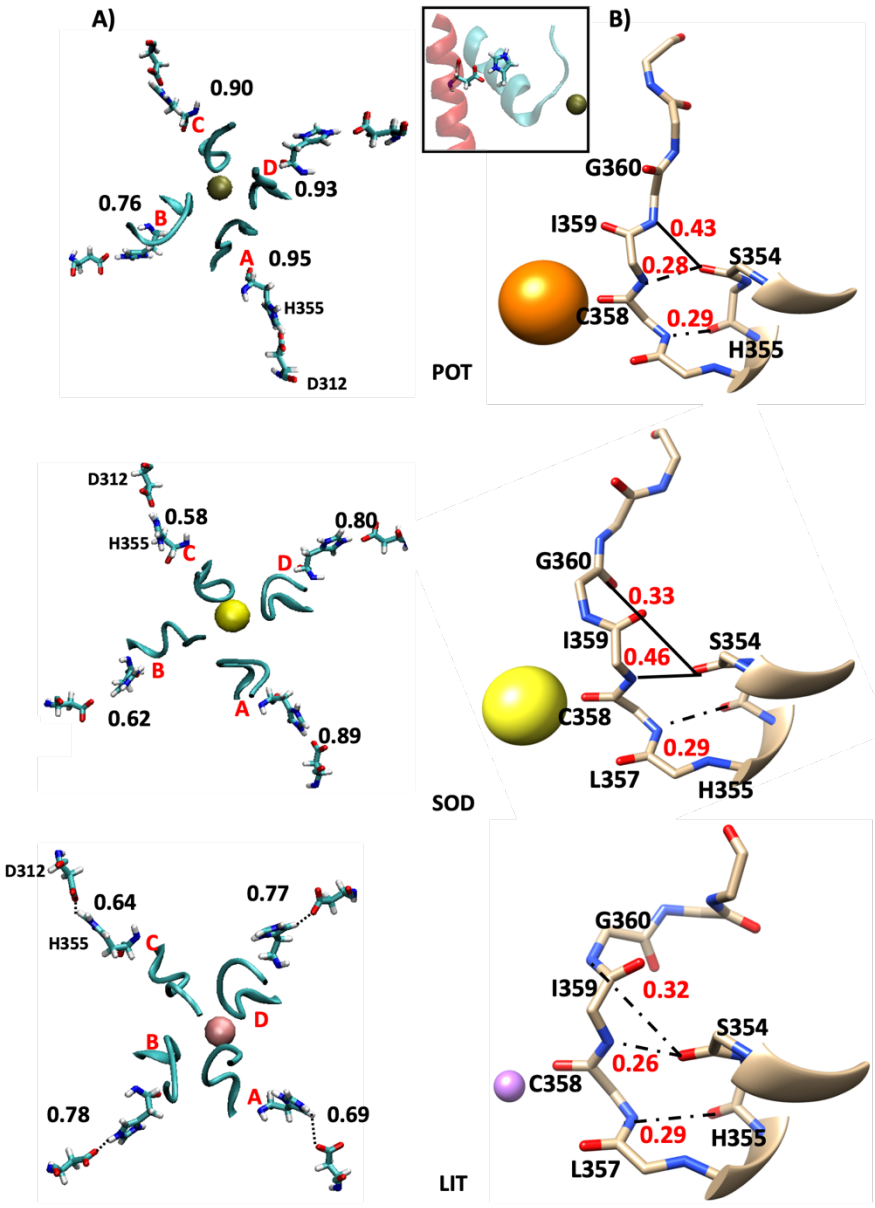

Figure 4. Hydrogen bond and electrostatic interactions behind the HCN1 selectivity filter (A) The occupancy of hydrogen bond between the sidechain of D312 and H\355 in the WT HCN1 systems. The pore is represented from the top view and the selectivity filter is represented as ribbon. Red letters indicate protein chains. The localization of D312 and H355 relative to selectivity filter is shown is the diagram confined in the box at the top of panel. **(B)** The average occupancy of hydrogen bond interaction between the mainchain residues of selectivity filter and the residues on the S5-S6 helix measured for the last 120 ns of the simulation. The stable location of ions during the simulation time are represented.

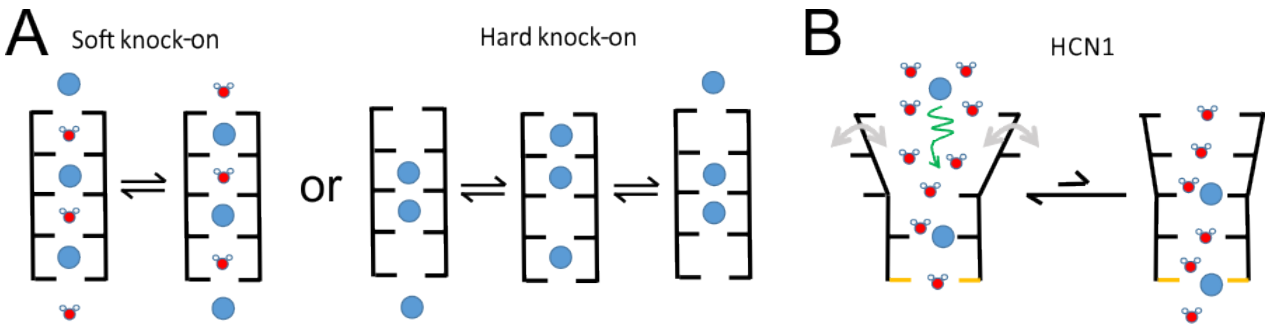

Figure 5. Permeation models of Kv and HCN channels. (A) Potassium channels have the backbone carbonyl groups of selectivity filter residues arranged in a cylindrical shape, gives rise to four equally spaced ion-binding sites known as S1-S4 sites from top to bottom. This symmetrical arrangement permits a K^+ ion to be coordinated by eight oxygen atoms from carbonyl groups of the selectivity filter with the ion sitting in the middle of a cubic cage. This synchronous coordination of K^+ ions in-turn helps the carbonyl groups remain oriented toward the conduction pathway and enables multiple K^+ ions to be coordinated in the pore, allowing for rapid ion conductance via "soft" of "hard" electrostatic repulsion (knock-on). **(B)** We propose the following model to explain ion permeation in HCN channels. The top of the HCN1 pore is highly flexible, favouring flipping of the carbonyl oxygens away from the central pore axis and preventing ion co-ordination. Therefore, only 1 ion stably binds in the HCN1 pore primarily in plane with the C358 carbonyl groups and into the S4 site. Infrequently, the top of the pore may achieve the proper orientation to co-ordinate a second ion in an outer site that can lead to electrostatic ion repulsion and permeation. However, the equilibrium favours the more disordered upper pore which contributes to low conductance (~1pS) in HCNs.

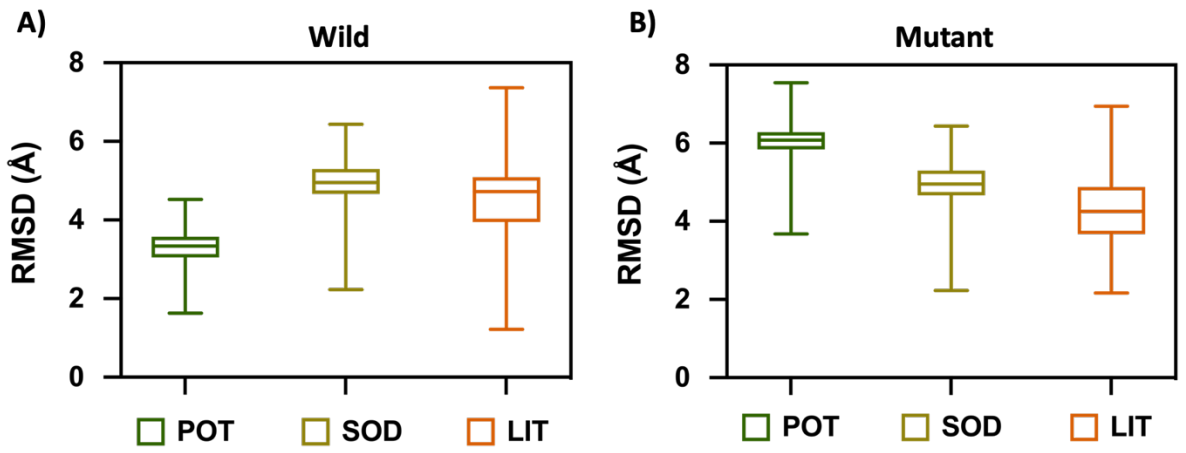

Figure S1. The box and whisker plot representing the distribution of RMSD for different ions during the last 120 ns of simulation. Each plot represents the median, lower quartile, upper quartile, lower extreme and upper extreme. The structure derived from the 80th ns of simulation was used as the reference structure to measure the RMSD. POT, SOD and LIT represent the K^+, Na^+ and Li^+ ions, respectively.

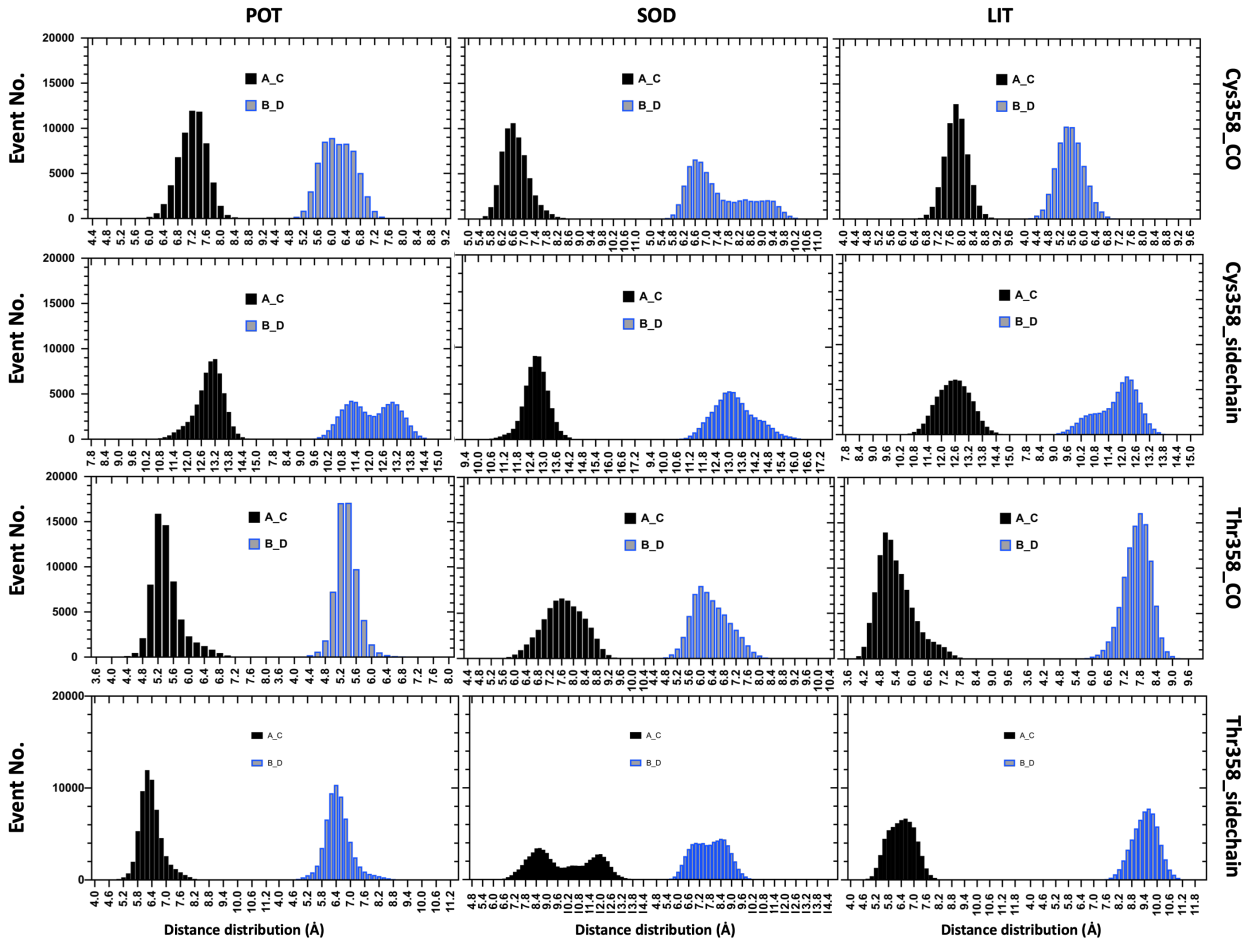

Figure S2. The histogram of the distribution of distance between the Sulfur/Oxygen atoms from the sidechain of opposing Cys358/Thr358 residues or the oxygen from the backbone of opposing Cys358/Thr358 residues, during the last 120 ns of simulation. The distances between chain A and C are represented by black color and the distances between chain B and D are represented by blue color. POT, SOD and LIT represent the K^+, Na^+ and Li^+ ions, respectively.

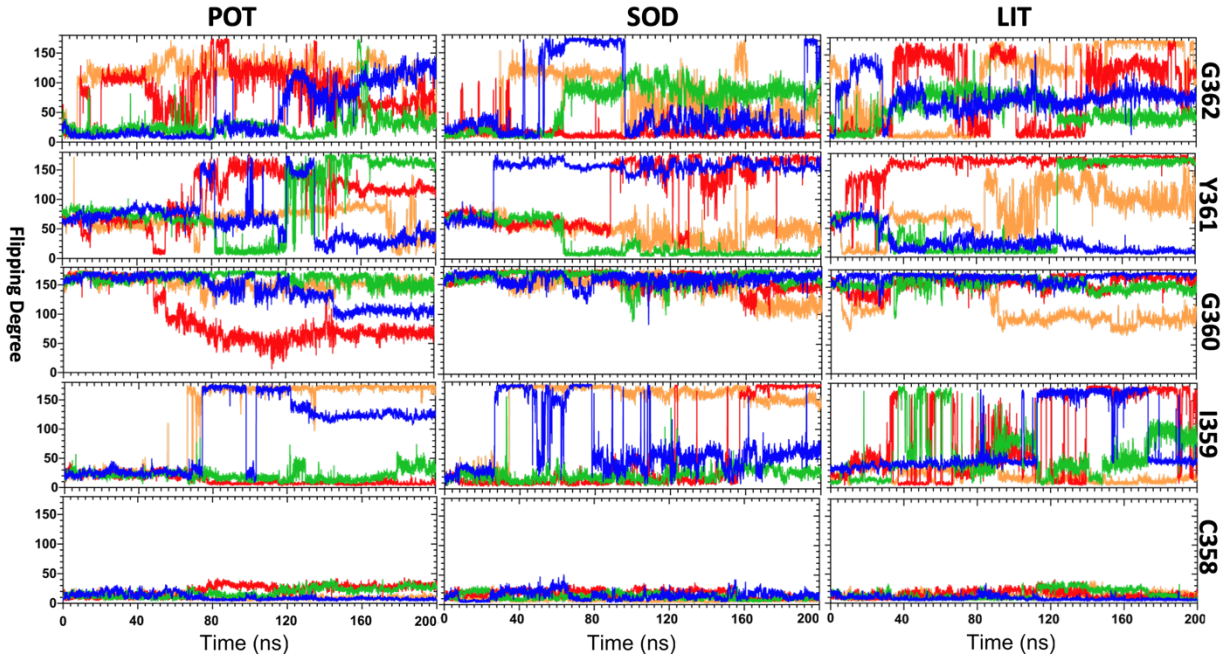

Figure S3. The degree flipping motions for the carbonyl group of the residues in the selectivity filter in the wildtype systems and during the simulation time. The color-coded diagrams represent the flipping motions of the tagged residues from chain A (blue), chain B (green), chain C (orange) and chain D (red) of the protein. POT, SOD and LIT represent the K^+, Na^+ and Li^+ ions, respectively.

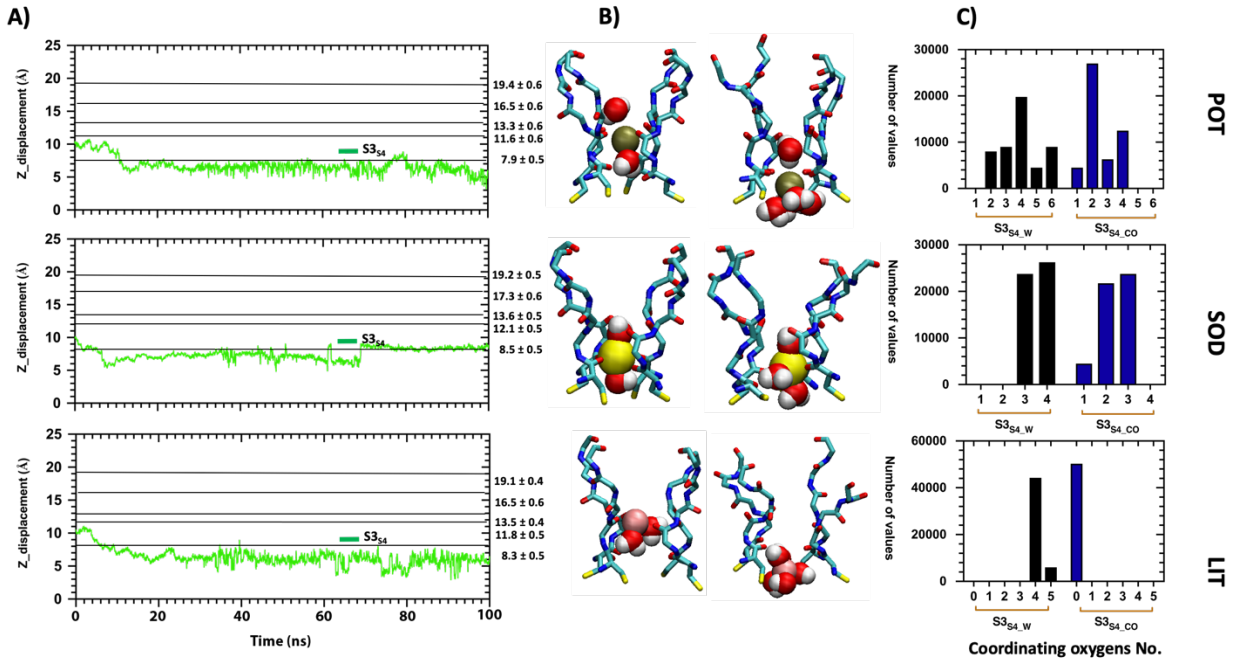

Figure S4. Trajectory of K^+ (POT), NA^+ (SOD) and Li^+ (LIT) ions in the selectivity filter of wildtype HCN1 when ions were initially placed only in the S3 site. A) The time evolution of K^+, Na^+ and Li^+ ions localization along the Z axis of selectivity filter through the simulation time are highlighted (green). The black diagrams represent the average geometrical localization of carbonyl groups of the selectivity filter residues. **B)** Snapshots of the selectivity filter taken at the start (*left*) and end (*right*) of the simulations indicate that the ions rapidly move from the S3 site into the S4 site and are co-ordinated similarly to what we observed in our other simulated systems. **C)** Histogram for the distribution of number of coordinating oxygens (from coordinating water molecules or backbone of selectivity filter residues) that coordinate each ion during the simulation. The captions under each graph represent the ion number and its location in the selectivity filter; $S3_{S4\_W}$ represents water molecules that coordinate the ion initially localized at S3 and translocated to S4 site during the simulation. $S3_{S4\_CO}$ represents carbonyl groups that directly coordinate the ion initially localized at S3 and translocated to S4 site during the simulation.

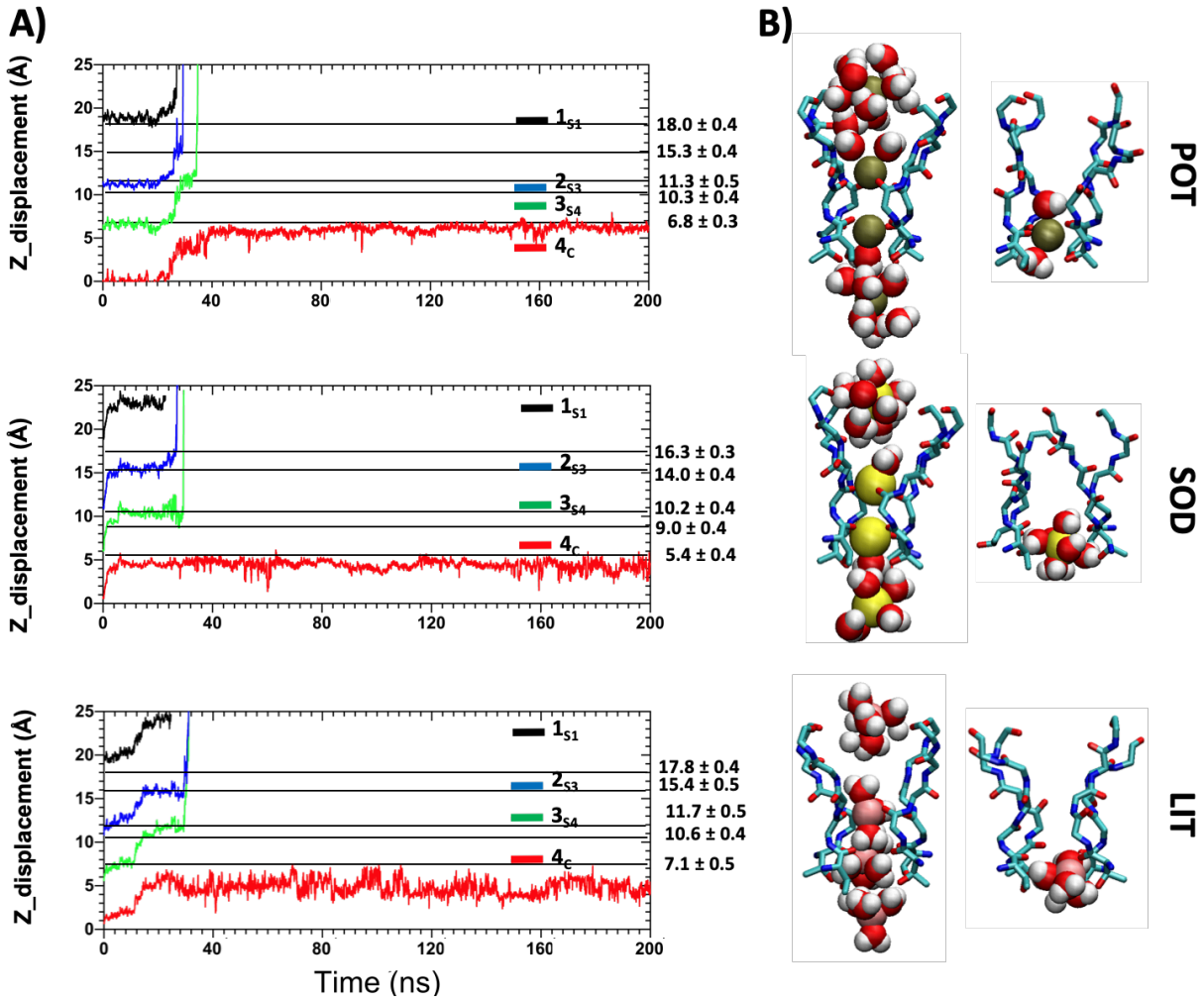

Figure S5. A single stable binding site for K^+ (POT), Na^+ (SOD) and Li^+ (LIT) ions in the C358T HCN1 selectivity filter (A) Trajectory of K^+, Na^+ and Li^+ ions localization along the Z axis of selectivity filter over the time-course of the simulations. The geometrical localization of each ion within different zones of selectivity filter are highlighted by different colors. 1_{S1} (black) represents the ion number 1 which was initially positioned in S1 site. 2_{S3} (blue) represents the ion number 2 which was initially positioned in S3 site. 3_{S4} (green) represents the ion number 3 which was initially positioned in S4 site. 4_C (red) represents the ion number 4 which was initially positioned in bottom cavity site. The thin black lines in the background of each graph represents the average location carbonyl groups in the selectivity filter along the Z axis (from bottom to top: C358T, I359, G360, Y361 and G362), with the specific values reported on the side of the graph. **(B)** Snapshots of the HCN1 selectivity filter with ions and their coordinating waters taken from the 20th ns, 100th ns and 200th ns, respectively.

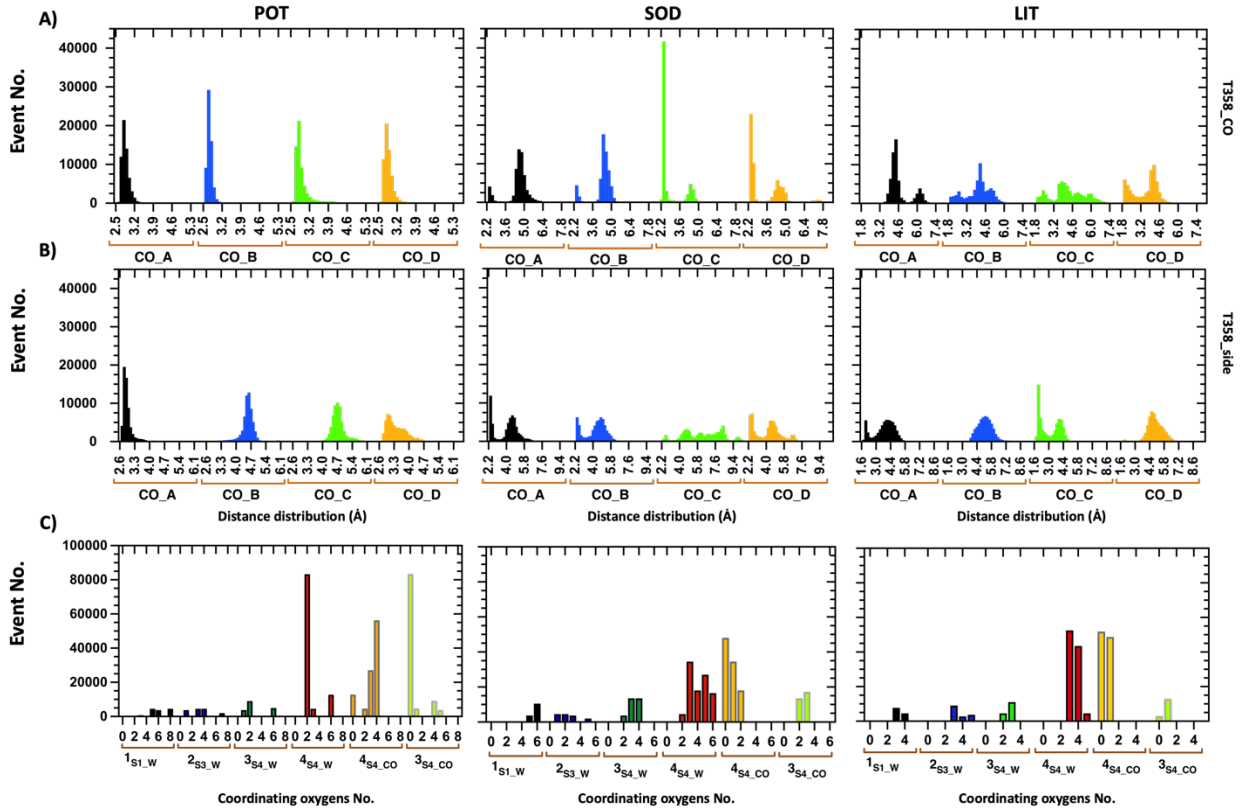

Figure S6. A) and B) Histogram for the distribution of distance (Å) between each ion and its coordinating oxygen atoms (from CO groups of Thr358 or its sidechain). The caption under each graph represents the distribution of aforementioned distances for each protein chain. **C)** Histogram for the distribution of oxygen atom numbers (from coordinating water molecules or backbone of selectivity filter residues) that coordinate each ion during the simulation. The captions under each graph represent the ion number and its location in the selectivity filter; 1_{S1_W} represents water molecules that coordinate ion number 1 initially localized at S1 site. 2_{S3_W} represents water molecules that coordinate ion number 2 initially localized at S3 site. 3_{S4_W} represents water molecules that coordinate ion number 3 initially localized at S4 site. 4_{S4_W} represents water molecules that coordinate ion number 4 following its translocation to S4 site. 4_{S4_CO} represents carbonyl groups that coordinate ion number 4 following its translocation to S4 site. 3_{S4_CO} represents carbonyl groups that coordinate ion number 3 while localized at S4 site.

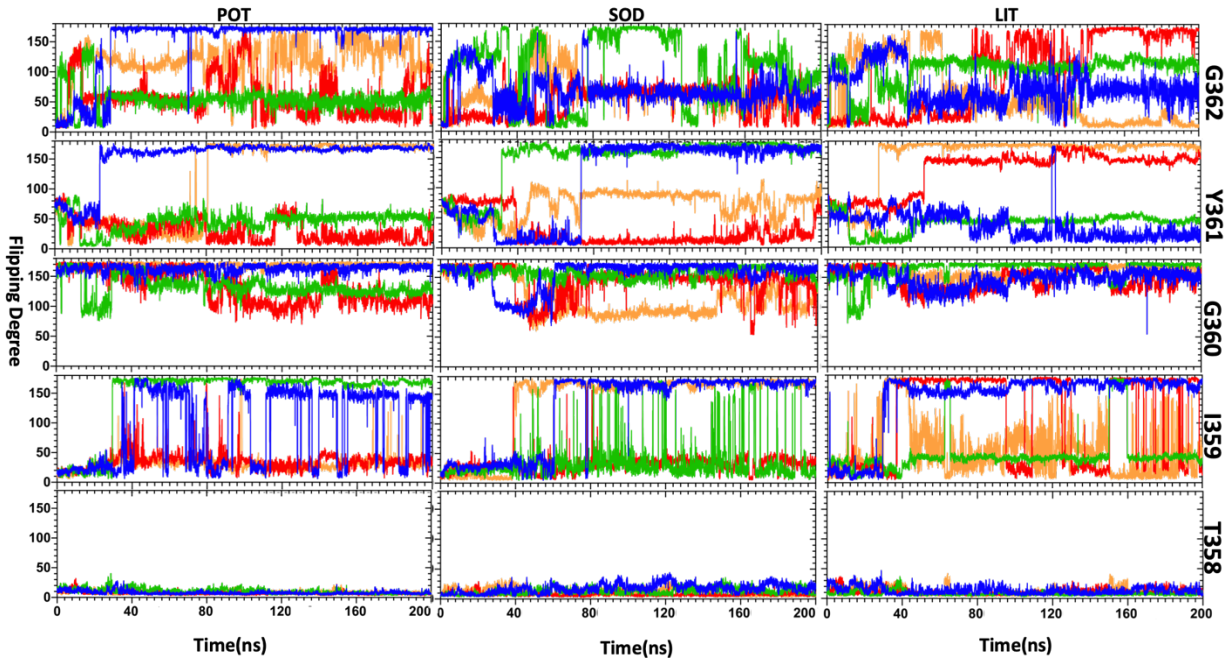

Figure S7. The degree flipping motions for the carbonyl group of the residues in the selectivity filter of HCN1 C358T mutant during the simulation time. The color-coded diagrams represent the flipping motions of the tagged residues from chain A (blue), chain B (green), chain C (orange) and chain D (red) of the protein. POT, SOD and LIT represent the K^+, Na^+ and Li^+ ions, respectively.

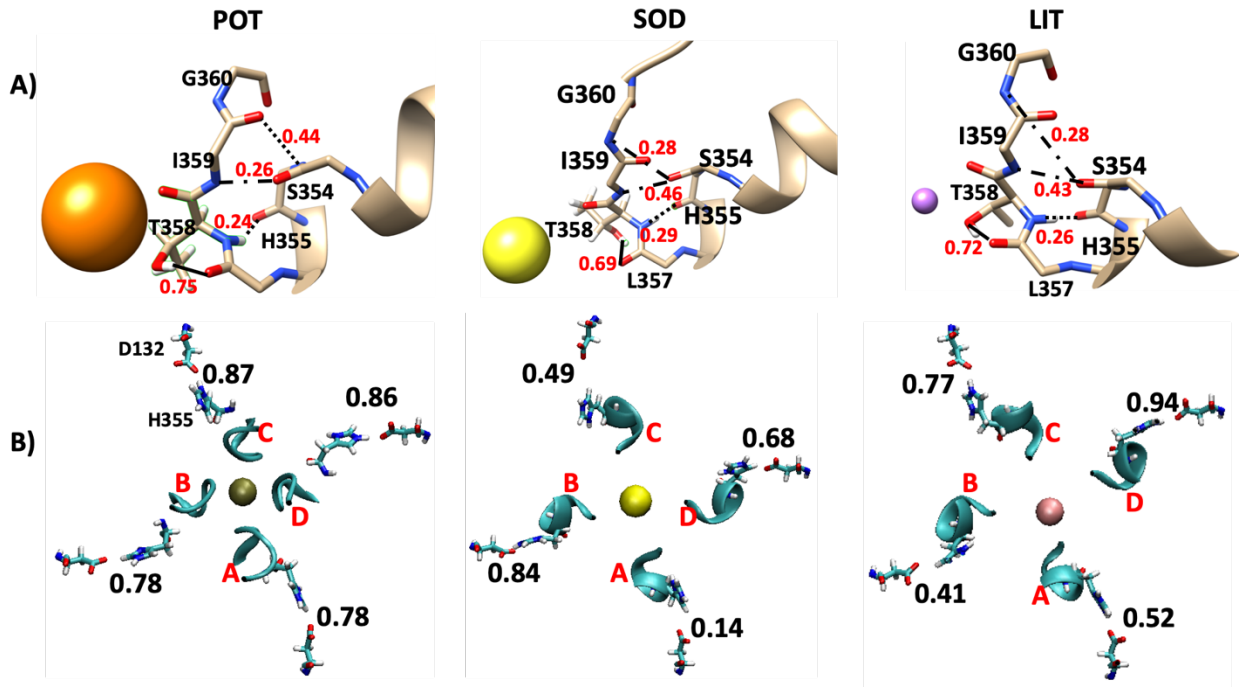

Figure S8. A) The average occupancy of hydrogen bond interaction between the mainchain residues of selectivity filter and the residues on the pore helix, in the mutated systems. The stable location of ions during the simulation time are represented. **B)** The occupancy of hydrogen bond between the sidechain of D312 and H355 in the mutated systems. The pore is represented from the top view and the selectivity filter is represented as ribbon. Red letters indicate protein chains. The localization of D312 and H355 relative to selectivity filter is shown is the diagram confined in the box at the top of panel. The hydrogen bond occupancies were measured for the last 120 ns of the simulation.

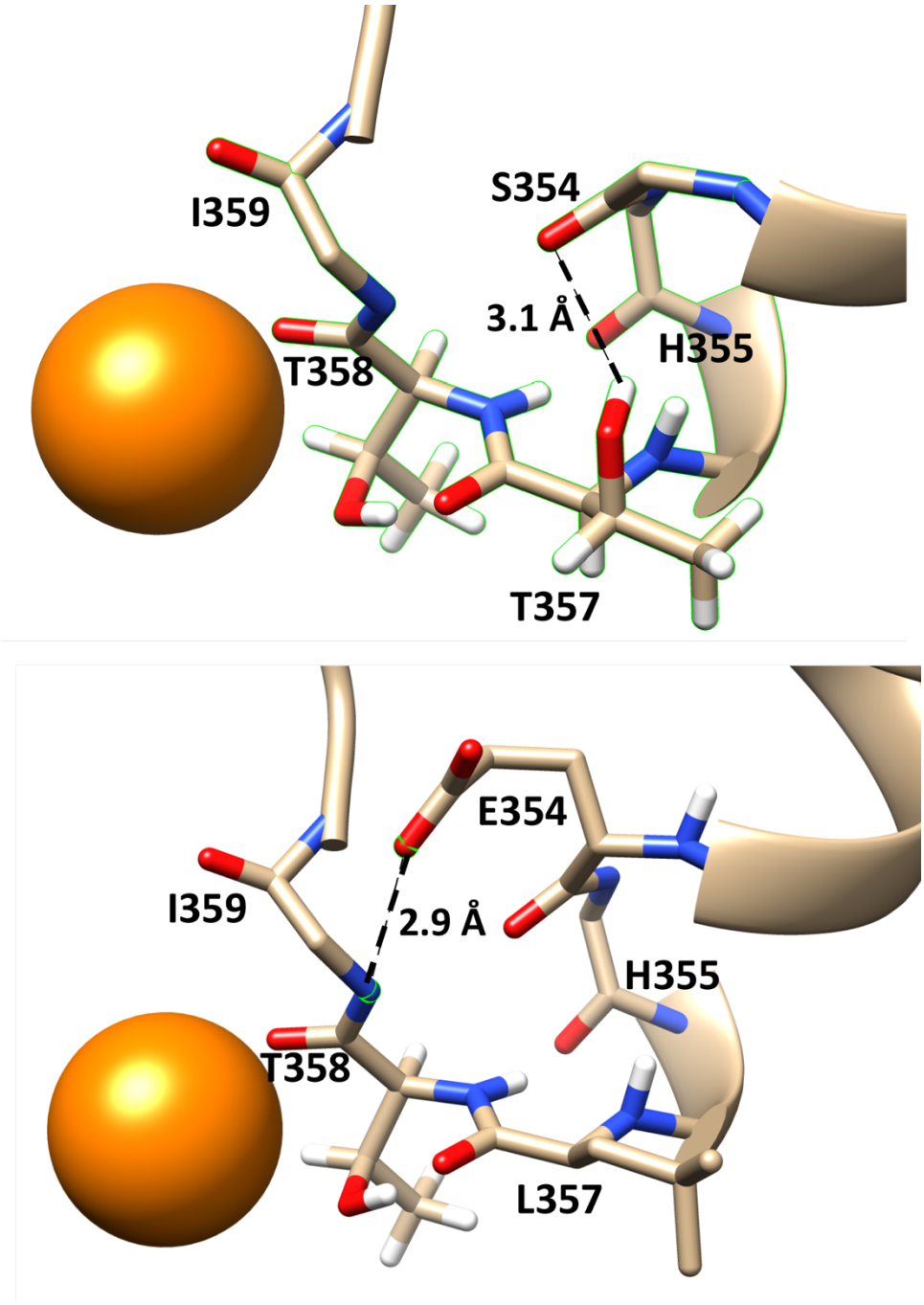

Figure S9. Structural model on Thr357 (top panel) and Glu354 (bottom panel) localization upon L357T and S354E point mutations. The new hydrogen bonds formed upon these mutations and the distance of interacting atoms are highlighted. The models were built by Rotamer tools of USCF Chimera [43] and the rotamers with minimum energy were selected for depiction.

References

1. Pape, H.C. Queer current and pacemaker: the hyperpolarization-activated cation current in neurons. *Annu Rev Physiol* **58**, 299-327 (1996).
2. Nolan, M.F. et al. The hyperpolarization-activated HCN1 channel is important for motor learning and neuronal integration by cerebellar Purkinje cells. *Cell* **115**, 551-64 (2003).
3. Nolan, M.F. et al. A behavioral role for dendritic integration: HCN1 channels constrain spatial memory and plasticity at inputs to distal dendrites of CA1 pyramidal neurons. *Cell* **119**, 719-32 (2004).
4. Emery, E.C., Young, G.T., Berrocoso, E.M., Chen, L. & McNaughton, P.A. HCN2 ion channels play a central role in inflammatory and neuropathic pain. *Science* **333**, 1462-6 (2011).
5. Stevens, D.R. et al. Hyperpolarization-activated channels HCN1 and HCN4 mediate responses to sour stimuli. *Nature* **413**, 631-5 (2001).
6. Knop, G.C. et al. Light responses in the mouse retina are prolonged upon targeted deletion of the HCN1 channel gene. *Eur J Neurosci* **28**, 2221-30 (2008).
7. Yancy, C.W. et al. 2017 ACC/AHA/HFSA focused update of the 2013 ACCF/AHA guideline for the management of heart failure: a report of the American College of Cardiology/American Heart Association Task Force on Clinical Practice Guidelines and the Heart Failure Society of America. *Journal of the American College of Cardiology* **70**, 776-803 (2017).
8. Cao, Y., Pang, J. & Zhou, P. HCN channel as therapeutic targets for heart failure and pain. *Current topics in medicinal chemistry* **16**, 1855-1861 (2016).
9. Santoro, B. & Shah, M.M. Hyperpolarization-activated cyclic nucleotide-gated channels as drug targets for neurological disorders. *Annual Review of Pharmacology and Toxicology* **60**, 109-131 (2020).
10. Yu, F.H., Yarov-Yarovoy, V., Gutman, G.A. & Catterall, W.A. Overview of molecular relationships in the voltage-gated ion channel superfamily. *Pharmacol Rev* **57**, 387-95 (2005).
11. Lee, C.H. & MacKinnon, R. Voltage Sensor Movements during Hyperpolarization in the HCN Channel. *Cell* **179**, 1582-1589 e7 (2019).
12. Lee, C.H. & MacKinnon, R. Structures of the Human HCN1 Hyperpolarization-Activated Channel. *Cell* **168**, 111-120 e11 (2017).
13. Porro, A. et al. The HCN domain couples voltage gating and cAMP response in hyperpolarization-activated cyclic nucleotide-gated channels. *Elife* **8**(2019).
14. Yu, H., Chang, F. & Cohen, I.S. Pacemaker current i (f) in adult canine cardiac ventricular myocytes. *The Journal of physiology* **485**, 469-483 (1995).
15. Hestrin, S. The properties and function of inward rectification in rod photoreceptors of the tiger salamander. *The Journal of physiology* **390**, 319-333 (1987).
16. Li, M. et al. Structure of a eukaryotic cyclic-nucleotide-gated channel. *Nature* **542**, 60-65 (2017).
17. Lee, C.-H. & MacKinnon, R. Structures of the human HCN1 hyperpolarization-activated channel. *Cell* **168**, 111-120. e11 (2017).

18. D'Avanzo, N., Pekhletski, R. & Backx, P.H. P-Loop Residues Critical for Selectivity in K+ Channels Fail to Confer Selectivity to Rabbit HCN4 Channels. *PloS one* **4**(2009).
19. Macri, V., Angoli, D. & Accili, E.A. Architecture of the HCN selectivity filter and control of cation permeation. *Scientific reports* **2**, 1-8 (2012).
20. Doyle, D.A. et al. The structure of the potassium channel: molecular basis of K+ conduction and selectivity. *science* **280**, 69-77 (1998).
21. Noskov, S.Y. & Roux, B. Ion selectivity in potassium channels. *Biophysical chemistry* **124**, 279-291 (2006).
22. DiFrancesco, D. Characterization of single pacemaker channels in cardiac sino-atrial node cells. *Nature* **324**, 470-473 (1986).
23. Lamoureux, G. & Roux, B. Absolute hydration free energy scale for alkali and halide ions established from simulations with a polarizable force field. *J Phys Chem B* **110**, 3308-22 (2006).
24. Cordero-Morales, J.F. et al. Molecular determinants of gating at the potassium-channel selectivity filter. *Nature structural & molecular biology* **13**, 311-318 (2006).
25. Cordero-Morales, J.F. et al. Molecular driving forces determining potassium channel slow inactivation. *Nature structural & molecular biology* **14**, 1062-1069 (2007).
26. Jekhmane, S. et al. Shifts in the selectivity filter dynamics cause modal gating in K+ channels. *Nature communications* **10**, 1-12 (2019).
27. Bezanilla, F. & Armstrong, C.M. Negative conductance caused by entry of sodium and cesium ions into the potassium channels of squid axons. *The Journal of General Physiology* **60**, 588-608 (1972).
28. Roux, B. Ion channels and ion selectivity. *Essays in biochemistry* **61**, 201-209 (2017).
29. Yu, H., Noskov, S.Y. & Roux, B. Two mechanisms of ion selectivity in protein binding sites. *Proceedings of the National Academy of Sciences* **107**, 20329-20334 (2010).
30. Noskov, S.Y. & Roux, B. Importance of hydration and dynamics on the selectivity of the KcsA and NaK channels. *The Journal of general physiology* **129**, 135-143 (2007).
31. Hille, B. Ion channels of excitable membranes. Sinauer Associates. *Sunderland, MA* **814**(2001).
32. Derebe, M.G. et al. Tuning the ion selectivity of tetrameric cation channels by changing the number of ion binding sites. *Proceedings of the National Academy of Sciences* **108**, 598-602 (2011).
33. Lockless, S.W. Determinants of cation transport selectivity: Equilibrium binding and transport kinetics. *Journal of General Physiology* **146**, 3-13 (2015).
34. Shi, N., Ye, S., Alam, A., Chen, L. & Jiang, Y. Atomic structure of a Na+-and K+-conducting channel. *Nature* **440**, 570-574 (2006).
35. Napolitano, L.M.R. et al. A structural, functional, and computational analysis suggests pore flexibility as the base for the poor selectivity of CNG channels. *Proceedings of the National Academy of Sciences* **112**, E3619-E3628 (2015).
36. Shrivastava, I.H., Tieleman, D.P., Biggin, P.C. & Sansom, M.S. K+ versus Na+ ions in a K channel selectivity filter: a simulation study. *Biophysical journal* **83**, 633-645 (2002).
37. Ludwig, A., Zong, X., Jeglitsch, M., Hofmann, F. & Biel, M. A family of hyperpolarization-activated mammalian cation channels. *Nature* **393**, 587-91 (1998).

38. Lacroix, J.J., Campos, F.V., Frezza, L. & Bezanilla, F. Molecular bases for the asynchronous activation of sodium and potassium channels required for nerve impulse generation. *Neuron* **79**, 651-657 (2013).
39. Favre, I., Moczydlowski, E. & Schild, L. On the structural basis for ionic selectivity among Na+, K+, and Ca2+ in the voltage-gated sodium channel. *Biophysical journal* **71**, 3110-3125 (1996).
40. Azene, E.M., Xue, T. & Li, R.A. Molecular basis of the effect of potassium on heterologously expressed pacemaker (HCN) channels. *J Physiol* **547**, 349-56 (2003).
41. Machado-Vieira, R., Manji, H.K. & Zarate Jr, C.A. The role of lithium in the treatment of bipolar disorder: convergent evidence for neurotrophic effects as a unifying hypothesis. *Bipolar disorders* **11**, 92-109 (2009).
42. Wainger, B.J., DeGennaro, M., Santoro, B., Siegelbaum, S.A. & Tibbs, G.R. Molecular mechanism of cAMP modulation of HCN pacemaker channels. *Nature* **411**, 805-810 (2001).
43. Pettersen, E.F. et al. UCSF Chimera--a visualization system for exploratory research and analysis. *J Comput Chem* **25**, 1605-12 (2004).
44. Olsson, M.H., Søndergaard, C.R., Rostkowski, M. & Jensen, J.H. PROPKA3: consistent treatment of internal and surface residues in empirical p K a predictions. *Journal of chemical theory and computation* **7**, 525-537 (2011).
45. Lomize, M.A., Lomize, A.L., Pogozheva, I.D. & Mosberg, H.I. OPM: orientations of proteins in membranes database. *Bioinformatics* **22**, 623-5 (2006).
46. Jo, S., Kim, T., Iyer, V.G. & Im, W. CHARMM-GUI: a web-based graphical user interface for CHARMM. *J Comput Chem* **29**, 1859-65 (2008).
47. Best, R.B. et al. Optimization of the additive CHARMM all-atom protein force field targeting improved sampling of the backbone phi, psi and side-chain chi(1) and chi(2) dihedral angles. *J Chem Theory Comput* **8**, 3257-3273 (2012).
48. Jorgensen, W.L., Chandrasekhar, J., Madura, J.D., Impey, R.W. & Klein, M.L. Comparison of Simple Potential Functions for Simulating Liquid Water. *Journal of Chemical Physics* **79**, 926-935 (1983).
49. Roux, B. & Berneche, S. On the potential functions used in molecular dynamics simulations of ion channels. *Biophys J* **82**, 1681-4 (2002).
50. Essmann, U., Perera, L. & Berkowitz, M.L. A smooth particle mesh Ewald method. *J. Chem. Phys.* **103**, 8577 (1995).
51. Feller, S.E., Zhang, Y., Pastor, R.W. & Brooks, B.R. Constant pressure molecular dynamics simulation: the Langevin piston method. *The Journal of Chemical Physics* **103**, 4613-4612 (1995).
52. Humphrey, W., Dalke, A. & Schulten, K. VMD: visual molecular dynamics. *J Mol Graph* **14**, 33-8, 27-8 (1996).

5- Discussion

HCN channels are semi-selective ion channels that permeate the K^+ over Na^+ ions almost to a 1:4 ratio. However, they are relatively impermeable to Li^+ ions. The structural details of the mechanism of selectivity in these channels is unknown and there is no structural data pertaining the precise localization of the ions in the selectivity filter as well as the atomistic details of protein-ion interaction.

We therefore modeled the structure HCN1 in the presence of either K^+, Na^+ or Li^+ ions to study the structural interactions that might explain the channel selectivity as well as the nature of selectivity filter dynamics in the presence of these ions. The initial structure of the simulation was derived from cryo-EM structure of the channel represented in its closed state. In following lines, the findings of the study will be discussed in the light of previous findings on the selectivity mechanism of related ion channels.

5.1- Dynamics of selectivity filter in HCN1 channel

According to the cryo-EM structure of HCN1 channel which was used as the template for modeling the structure in the presence of ions (PDB code: 5U6O), the selectivity filter assumes a funnel shape from top to bottom. In this conformation, the carbonyl groups of the Cys358 and Ile359 are pointed toward the interior of the selectivity filter while the carbonyl groups of the three top residues (Gly360, Tyr361 and Gly362) are disoriented and unable to coordinate the ion. Based on this observation, it is suggested that probably two binding sites exists in this channel at S3 and S4 sites. However, the selectivity filter is relatively dilatated at these two sites with around 5Å distance between the opposing oxygen atoms of the coordinating. Upon the simulation, this distance fluctuates according to the nature of ion being present in the selectivity filter and expands up to 12 Å. Additionally, the S3 binding site is lost due to flipping motions of Ile359 carbonyl groups. In case of the CNG channel, the closest relative to HCN channels, the selectivity filter has a more or less a cylindrical structure and based on the crystal structure of the protein, holds three binding sites for the ion binding (PDB code: 5H3O)[82]. Similar to HCN1 channel, the pore is relatively dilatated in CNG channel and the diameter of the opposing oxygens that coordinate the

ion ranges between 7Å to 9.5Å [82]. It has been argued that this conformation of selectivity filter would allow ions with one or more hydration waters to pass, consistent with the poor monovalent cation selectivity of CNG channels. Such explanation could also justify the poor selectivity of HCN channels. However, it may worth reminding that HCNs have week selectivity for Na^+ ions over K^+. Our simulation results is suggestive of relatively tighter and more ordered selectivity filter conformation in the presence of the K^+ ions in the filter. However, these differences are negligible and regarding the stochastic nature of MD simulation, should be interpreted with caution.

Our data suggest that the selectivity filter dynamics and ion localization could have mutual effects on each other and in order to explain the mechanism of selectivity three factors should be accounted simultaneously; (i) the dynamics and conformation of the selectivity filter, (ii) the diameter of the ion being present in the pore and (iii) the dehydration energy of each ion. Considering these notions, it seems that the pore prepares the best environment for both K^+ followed by Na^+. The highly dynamic nature of the selectivity filter results in drastic fluctuations of its diameter. The K^+ ion can fit in this varied environment by fluctuating between different hydrating states which is more affordable considering its dehydration energy compared to Na+ and Li^+. This may justify the observed selectivity pattern of the channels against these cations.

5.2- Ion localization in selectivity filter of HCN1 channel

According to our simulation results, only one ion is stably localized in the selectivity filter. Interestingly, this ion is mostly localized either between the carbonyl groups of Cys358 or S4 site. To the best of our knowledge, such pattern of ion localization in selectivity filter has not been reported in case of any other channel. A similar pattern was also observed in our other set of simulations performed with one ion in the selectivity filter which was initially localized in S3 site. In this regard, it seems that the nature of selectivity of HCN against K^+, Na^+ and Li^+ ions is pretty much dependent on the conformational dynamics and size of the S4 site. This view can justify why the selectivity against Li^+ ion is lost upon C358T mutation;

According to our simulation results, the S4 site is wide open in the wildtype structure as the result of distant localization of Cys358 sidechains. This spacious S4 site allows for radical fluctuations of Li^+ ion and hence its compromised coordination. However, upon the C358T mutation, this space

becomes more confined due to localization of Thr358 sidechains to a closer proximity of the ion. This in turn could lead to more restricted ion movement and better coordination of the ion.

5.3- Network of Hydrogen bonds between selectivity filter and pore helix

Previous studies have highlighted the role interactions between selectivity filter and the pore helix in regulating the selectivity filter fluidity and its ability to coordinate the permeating ions. in case of CNG channels which are considered non-selective channels, the nature of interactions between the selectivity filter and the pore helix are mostly hydrophobic. These greasy hydrophobic interaction have been suggested as the base of selectivity filter flexibility and lack of selectivity [82]. Unlike the CNG channels, the corresponding interactions in HCN1 channel have an electrostatic nature. According to our simulation results, this network mainly exists between the residues at the bottom of the pore and the base of pore helix. It seems that despite the lack stringency, these interactions are strong enough to impart some levels of rigidity to the lower regions of the selectivity filter and probably contribute to the week selectivity of Na^+ ions over K^+ ions.

5.4- Limitations of the study

5.4.1- Using the closed conformation of the channel

In this study the interaction of ions with HCN1 protein was modeled based on the structure of cryo-EM structure of the channel in the closed state. Recently the cryo-EM structure of the open conformation of HCN1 channel was also made available. The least square fitting of the open and closed conformations suggests for negligible difference in the selectivity filter conformation. In this study, we observed that except for the ion trapped in S4 site, the other ions pop out the pore and into the extracellular space. However, there is a chance that the ions move in the opposite direction if the open conformation of the channel is utilized. Despite this and considering the similarity of selectivity filter conformation in both open and closed conformations, it is probable that a similar pattern be observed for the stable ion localization in the selectivity filter.

5.4.2- The time period of simulation

The other limitation of our study is related to relatively short time of simulation. Considering the symmetrical arrangement of the pore, it is expected that all subunits behave similarly along the simulation time. This is more or less true in case of the current study. However, if the simulation is prolonged, those interactions related to hydrogen bonds between the selectivity filter and the pore helix would converge in all the subunits and show a cleaner pattern.

5.5- Future directions

5.5.1- Site-directed mutagenesis studies to manipulate selectivity filter dynamics

In addition to validating the findings in the open model of the channel as well as prolonging the simulation time, we suggest several experimental tests to evaluate the role of hydrogen bond network behind the selectivity filter in regulating the selectivity filter dynamics as well as the selectivity features of the channel;

As mentioned in the results, the network of hydrogen bond between the selectivity filter and the pore helix mainly exists for the bottom residues of the selectivity filter and at the top, selectivity filter residues are free to move with no engagement to pore helix residues. A closer look at this zone and in comparison, with highly selective Kv channels suggest that two simultaneous mutations could restore this hydrogen bond with the top of selectivity filter to some extent. The A363D and F351W could induce the hydrogen bond between Asp363 and Trp35 and restore the conventional hydrogen bond network at the top of the selectivity filter. This, in turn could lead to more stable conformation of the selectivity filter and partial to full restoration of the S1, S2 and S3 binding sites. This hypothesis could be tested through a combination of experimental and computational approaches such as site directed mutagenesis electrophysiology recordings as well as MD simulation.

6- Conclusion

In this study we evaluated the structural dynamics of the selectivity filter in HCN1 channel and in the presence of K^+, Na^+ and Li^+. Our data suggest that there is one stable binding site for the ion in the vicinity of the S4 site. The backbone of the selectivity filter at this binding site is reinforced through a network of hydrogen bonds between the selectivity filter and the pore helix. Our data also suggest that K^+ and Na^+ can better fit in this flexible binding site due to their larger size and the fact that they can partially be stripped from their coordination water molecules and directly interact with the carbonyl groups of Cys358. However, in case of Li^+, the ion is strongly shielded by water molecules and fail to be directly coordinated by the carbonyl groups of Cys358. Therefore, it is descended to the S4 site where it radically wanders in the wide open S4 cavity. The C358T mutation seems to confine the Li^+ in the S4 site and increases the chance of its synchronous coordination by carbonyl groups of the selectivity filter.

7- Bibliography

References

1 Larsson, H. P. How is the heart rate regulated in the sinoatrial node? Another piece to the puzzle. *Journal of General Physiology* **136**, 237-241 (2010).

2 DiFrancesco, J. C. & DiFrancesco, D. Dysfunctional HCN ion channels in neurological diseases. *Frontiers in cellular neuroscience* **9**, 71 (2015).

3 Yancy, C. W. *et al*. 2017 ACC/AHA/HFSA focused update of the 2013 ACCF/AHA guideline for the management of heart failure: a report of the American College of Cardiology/American Heart Association Task Force on Clinical Practice Guidelines and the Heart Failure Society of America. *Journal of the American College of Cardiology* **70**, 776-803 (2017).

4 Frank, H. Y., Yarov-Yarovoy, V., Gutman, G. A. & Catterall, W. A. Overview of molecular relationships in the voltage-gated ion channel superfamily. *Pharmacological reviews* **57**, 387-395 (2005).

5 Lee, C.-H. & MacKinnon, R. Structures of the human HCN1 hyperpolarization-activated channel. *Cell* **168**, 111-120. e111 (2017).

6 Lee, C.-H. & MacKinnon, R. Voltage sensor movements during hyperpolarization in the HCN channel. *Cell* **179**, 1582-1589. e1587 (2019).

7 DiFrancesco, D. Pacemaker mechanisms in cardiac tissue. *Annual review of physiology* **55**, 455-472 (1993).

8 Brown, H. F. Electrophysiology of the sinoatrial node. *Physiological Reviews* **62**, 505-530 (1982).

9 Hauswirth, O., Noble, D. & Tsien, R. Adrenaline: mechanism of action on the pacemaker potential in cardiac Purkinje fibers. *Science* **162**, 916-917 (1968).

10 Noble, D. & Tsien, R. The kinetics and rectifier properties of the slow potassium current in cardiac Purkinje fibres. *The Journal of Physiology* **195**, 185-214 (1968).

11 Brown, H., DiFrancesco, D. & Noble, S. How does adrenaline accelerate the heart? *Nature* **280**, 235-236 (1979).

12 Klabunde, R. *Cardiovascular physiology concepts*. (Lippincott Williams & Wilkins, 2011).

13 Tulane_University. *introduction_to_cardiac_physiology_electrophysiology*, <http://tmedweb.tulane.edu/pharmwiki/doku.php/introduction_to_cardiac_physiology_electrophysiology> (2018).

14 Klabunde RE. *Cardiovascular Pharmacology Concepts*. *CV Pharmacology*, <https://www.cvpharmacology.com/antiarrhy/cardiac_action_potentials> (2006-2020).

15 Ludwig, A., Zong, X., Jeglitsch, M., Hofmann, F. & Biel, M. A family of hyperpolarization-activated mammalian cation channels. *nature* **393**, 587-591 (1998).

16 Santoro, B. *et al*. Identification of a gene encoding a hyperpolarization-activated pacemaker channel of brain. *Cell* **93**, 717-729 (1998).

17 Moosmang, S., Biel, M., Hofmann, F. & Ludwig, A. Differential distribution of four hyperpolarization-activated cation channels in mouse brain. *Biological chemistry* **380**, 975-980 (1999).

18 Notomi, T. & Shigemoto, R. Immunohistochemical localization of Ih channel subunits, HCN1–4, in the rat brain. *Journal of Comparative Neurology* **471**, 241-276 (2004).

19 He, C., Chen, F., Li, B. & Hu, Z. Neurophysiology of HCN channels: from cellular functions to multiple regulations. *Progress in neurobiology* **112**, 1-23 (2014).

20 Shah, M. M. Hyperpolarization-activated cyclic nucleotide-gated channel currents in neurons. *Cold Spring Harbor Protocols* **2016**, pdb. top087346 (2016).

21 Magee, J. C. & Johnston, D. Plasticity of dendritic function. *Current opinion in neurobiology* **15**, 334-342 (2005).

22 Lörincz, A., Notomi, T., Tamás, G., Shigemoto, R. & Nusser, Z. Polarized and compartment-dependent distribution of HCN1 in pyramidal cell dendrites. *Nature neuroscience* **5**, 1185-1193 (2002).

23 Williams, S. R. & Stuart, G. J. Site independence of EPSP time course is mediated by dendritic I h in neocortical pyramidal neurons. *Journal of neurophysiology* **83**, 3177-3182 (2000).

24 Magee, J. C. & Cook, E. P. Somatic EPSP amplitude is independent of synapse location in hippocampal pyramidal neurons. *Nature neuroscience* **3**, 895-903 (2000).

25 Fernandes, D. & Carvalho, A. L. Mechanisms of homeostatic plasticity in the excitatory synapse. *Journal of neurochemistry* **139**, 973-996 (2016).

26 Fan, Y. *et al*. Activity-dependent decrease of excitability in rat hippocampal neurons through increases in I h. *Nature neuroscience* **8**, 1542-1551 (2005).

27 Nolan, M. F. *et al*. A behavioral role for dendritic integration: HCN1 channels constrain spatial memory and plasticity at inputs to distal dendrites of CA1 pyramidal neurons. *Cell* **119**, 719-732 (2004).

28 Tsay, D., Dudman, J. T. & Siegelbaum, S. A. HCN1 channels constrain synaptically evoked Ca2+ spikes in distal dendrites of CA1 pyramidal neurons. *Neuron* **56**, 1076-1089 (2007).

29 Lüthi, A. & McCormick, D. A. H-current: properties of a neuronal and network pacemaker. *Neuron* **21**, 9-12 (1998).

30 Jiang, Y.-Q., Sun, Q., Tu, H.-Y. & Wan, Y. Characteristics of HCN channels and their participation in neuropathic pain. *Neurochemical research* **33**, 1979-1989 (2008).

31 Emery, E. C., Young, G. T., Berrocoso, E. M., Chen, L. & McNaughton, P. A. HCN2 ion channels play a central role in inflammatory and neuropathic pain. *Science* **333**, 1462-1466 (2011).

32 Tibbs, G. R. *et al*. HCN1 channels as targets for anesthetic and nonanesthetic propofol analogs in the amelioration of mechanical and thermal hyperalgesia in a mouse model of

neuropathic pain. *Journal of Pharmacology and Experimental Therapeutics* **345**, 363-373 (2013).

33 Sartiani, L., Mannaioni, G., Masi, A., Romanelli, M. N. & Cerbai, E. The hyperpolarization-activated cyclic nucleotide–gated channels: from biophysics to pharmacology of a unique family of ion channels. *Pharmacological reviews* **69**, 354-395 (2017).

34 Poolos, N. P., Migliore, M. & Johnston, D. Pharmacological upregulation of h-channels reduces the excitability of pyramidal neuron dendrites. *Nature neuroscience* **5**, 767-774 (2002).

35 Baruscotti, M., Bottelli, G., Milanesi, R., DiFrancesco, J. C. & DiFrancesco, D. HCN-related channelopathies. *Pflügers Archiv-European Journal of Physiology* **460**, 405-415 (2010).

36 Huang, Z., Walker, M. C. & Shah, M. M. Loss of dendritic HCN1 subunits enhances cortical excitability and epileptogenesis. *Journal of Neuroscience* **29**, 10979-10988 (2009).

37 Santoro, B. *et al*. Increased seizure severity and seizure-related death in mice lacking HCN1 channels. *Epilepsia* **51**, 1624-1627 (2010).

38 DiFrancesco, J. C. *et al*. Recessive loss-of-function mutation in the pacemaker HCN2 channel causing increased neuronal excitability in a patient with idiopathic generalized epilepsy. *Journal of Neuroscience* **31**, 17327-17337 (2011).

39 Yi, F. *et al*. Autism-associated SHANK3 haploinsufficiency causes Ih channelopathy in human neurons. *Science* **352**, aaf2669 (2016).

40 Arnsten, A. F. Prefrontal cortical network connections: key site of vulnerability in stress and schizophrenia. *International Journal of Developmental Neuroscience* **29**, 215-223 (2011).

41 Paspalas, C. D., Wang, M. & Arnsten, A. F. Constellation of HCN channels and cAMP regulating proteins in dendritic spines of the primate prefrontal cortex: potential substrate for working memory deficits in schizophrenia. *Cerebral cortex* **23**, 1643-1654 (2013).

42 Cao, J.-L. *et al*. Mesolimbic dopamine neurons in the brain reward circuit mediate susceptibility to social defeat and antidepressant action. *Journal of Neuroscience* **30**, 16453-16458 (2010).

43 Lewis, A. S. *et al*. Deletion of the hyperpolarization-activated cyclic nucleotide-gated channel auxiliary subunit TRIP8b impairs hippocampal Ih localization and function and promotes antidepressant behavior in mice. *Journal of Neuroscience* **31**, 7424-7440 (2011).

44 Knoll, A. T., Halladay, L. R., Holmes, A. & Levitt, P. Quantitative trait loci and a novel genetic candidate for fear learning. *Journal of Neuroscience* **36**, 6258-6268 (2016).

45 Noda, M., Suzuki, H., Numa, S. & Stühmer, W. A single point mutation confers tetrodotoxin and saxitoxin insensitivity on the sodium channel II. *FEBS letters* **259**, 213-216 (1989).

46 Striessnig, J., Glossmann, H. & Catterall, W. A. Identification of a phenylalkylamine binding region within the alpha 1 subunit of skeletal muscle Ca2+ channels. *Proceedings of the National Academy of Sciences* **87**, 9108-9112 (1990).

47 MacKinnon, R. & Yellen, G. Mutations affecting TEA blockade and ion permeation in voltage-activated K+ channels. *Science* **250**, 276-279 (1990).

48 Hartmann, H. A. *et al*. Exchange of conduction pathways between two related K+ channels. *Science* **251**, 942-944 (1991).

49 Wang, G.-K. & Strichartz, G. State-dependent inhibition of sodium channels by local anesthetics: a 40-year evolution. *Biochemistry (Moscow) Supplement Series A: Membrane and Cell Biology* **6**, 120-127 (2012).

50 Hockerman, G. H., Johnson, B. D., Scheuer, T. & Catterall, W. A. Molecular determinants of high affinity phenylalkylamine block of L-type calcium channels. *Journal of Biological Chemistry* **270**, 22119-22122 (1995).

51 Moran, Y., Barzilai, M. G., Liebeskind, B. J. & Zakon, H. H. Evolution of voltage-gated ion channels at the emergence of Metazoa. *Journal of Experimental Biology* **218**, 515-525 (2015).

52 Doyle, D. A. *et al*. The structure of the potassium channel: molecular basis of K+ conduction and selectivity. *science* **280**, 69-77 (1998).

53 Bezanilla, F. The voltage sensor in voltage-dependent ion channels. *Physiological reviews* **80**, 555-592 (2000).

54 Glauner, K. S., Mannuzzu, L. M., Gandhi, C. S. & Isacoff, E. Y. Spectroscopic mapping of voltage sensor movement in the Shaker potassium channel. *Nature* **402**, 813-817 (1999).

55 Jiang, Y. *et al*. Crystal structure and mechanism of a calcium-gated potassium channel. *Nature* **417**, 515-522 (2002).

56 Jiang, Y. *et al*. The open pore conformation of potassium channels. *Nature* **417**, 523-526 (2002).

57 Biel, M., Wahl-Schott, C., Michalakis, S. & Zong, X. Hyperpolarization-activated cation channels: from genes to function. *Physiological reviews* **89**, 847-885 (2009).

58 Flynn, G. E. & Zagotta, W. N. Insights into the molecular mechanism for hyperpolarization-dependent activation of HCN channels. *Proceedings of the National Academy of Sciences* **115**, E8086-E8095 (2018).

59 Gauss, R., Seifert, R. & Kaupp, U. B. Molecular identification of a hyperpolarization-activated channel in sea urchin sperm. *Nature* **393**, 583-587 (1998).

60 Macri, V., Angoli, D. & Accili, E. A. Architecture of the HCN selectivity filter and control of cation permeation. *Scientific reports* **2**, 1-8 (2012).

61 Robinson, R. B. & Siegelbaum, S. A. Hyperpolarization-activated cation currents: from molecules to physiological function. *Annual review of physiology* **65**, 453-480 (2003).

62 Ho, W.-K., Brown, H. F. & Noble, D. High selectivity of the i f channel to Na+ and K+ in rabbit isolated sinoatrial node cells. *Pflügers Archiv* **426**, 68-74 (1994).

63 Santoro, B. & Tibbs, G. R. The HCN gene family: molecular basis of the hyperpolarization-activated pacemaker channels. *Annals of the New York Academy of Sciences* **868**, 741-764 (1999).

64 DiFrancesco, D. Characterization of single pacemaker channels in cardiac sino-atrial node cells. *Nature* **324**, 470-473 (1986).

65 Dekker, J. P. & Yellen, G. Cooperative gating between single HCN pacemaker channels. *The Journal of general physiology* **128**, 561-567 (2006).

66 Hille, B. Ionic channels of excitable membranes, Sinauer Assoc. *Inc., Sunderland, MA* (2001).

67 D'Avanzo, N., Pekhletski, R. & Backx, P. H. P-Loop Residues Critical for Selectivity in K+ Channels Fail to Confer Selectivity to Rabbit HCN4 Channels. *PloS one* **4** (2009).

68 Jekhmane, S. *et al*. Shifts in the selectivity filter dynamics cause modal gating in K+ channels. *Nature communications* **10**, 1-12 (2019).

69 Pless, S. A., Galpin, J. D., Niciforovic, A. P., Kurata, H. T. & Ahern, C. A. Hydrogen bonds as molecular timers for slow inactivation in voltage-gated potassium channels. *Elife* **2**, e01289 (2013).

70 Zhou, Y., Morais-Cabral, J. H., Kaufman, A. & MacKinnon, R. Chemistry of ion coordination and hydration revealed by a K+ channel–Fab complex at 2.0 Å resolution. *Nature* **414**, 43-48 (2001).

71 Ishii, T. M., Takano, M., Xie, L.-H., Noma, A. & Ohmori, H. Molecular characterization of the hyperpolarization-activated cation channel in rabbit heart sinoatrial node. *Journal of Biological Chemistry* **274**, 12835-12839 (1999).

72 Azene, E., Xue, T. & Li, R. A. Molecular basis of the effect of potassium on heterologously expressed pacemaker (HCN) channels. *The Journal of physiology* **547**, 349-356 (2003).

73 Coates, L. Ion permeation in potassium ion channels. *Acta Crystallographica Section D: Structural Biology* **76** (2020).

74 Roux, B. Ion channels and ion selectivity. *Essays in biochemistry* **61**, 201-209 (2017).

75 Chakrabarti, N. *et al*. Catalysis of Na+ permeation in the bacterial sodium channel NaVAb. *Proceedings of the National Academy of Sciences* **110**, 11331-11336 (2013).

76 Finol-Urdaneta, R. K. *et al*. Sodium channel selectivity and conduction: prokaryotes have devised their own molecular strategy. *Journal of General Physiology* **143**, 157-171 (2014).

77 Ing, C. & Pomes, R. in *Current topics in membranes* Vol. 78 215-260 (Elsevier, 2016).

78 Biel, M. Cyclic nucleotide-regulated cation channels. *Journal of Biological Chemistry* **284**, 9017-9021 (2009).

79 Kaupp, U. B. & Seifert, R. Cyclic nucleotide-gated ion channels. *Physiological reviews* **82**, 769-824 (2002).

80 Frings, S., Seifert, R., Godde, M. & Kaupp, U. B. Profoundly different calcium permeation and blockage determine the specific function of distinct cyclic nucleotide-gated channels. *Neuron* **15**, 169-179 (1995).

81 Yu, X. *et al*. Calcium influx through I f channels in rat ventricular myocytes. *American Journal of Physiology-Cell Physiology* **292**, C1147-C1155 (2007).

82 Li, M. *et al*. Structure of a eukaryotic cyclic-nucleotide-gated channel. *Nature* **542**, 60-65 (2017).

83 Derebe, M. G. *et al*. Tuning the ion selectivity of tetrameric cation channels by changing the number of ion binding sites. *Proceedings of the National Academy of Sciences* **108**, 598-602 (2011).

84 Lockless, S. W. Determinants of cation transport selectivity: Equilibrium binding and transport kinetics. *Journal of General Physiology* **146**, 3-13 (2015).

85 Shi, N., Ye, S., Alam, A., Chen, L. & Jiang, Y. Atomic structure of a Na+-and K+-conducting channel. *Nature* **440**, 570-574 (2006).

86 Huxley, A. Hodgkin and the action potential 1935–1952. *The Journal of physiology* **538**, 2 (2002).

87 Jensen, M. Ø. *et al*. Mechanism of voltage gating in potassium channels. *Science* **336**, 229-233 (2012).

88 Noskov, S. Y. & Roux, B. Ion selectivity in potassium channels. *Biophysical chemistry* **124**, 279-291 (2006).

89 Cooper, A. Thermodynamic fluctuations in protein molecules. *Proceedings of the National Academy of Sciences* **73**, 2740-2741 (1976).

90 Karplus, M., McCammon, J. A. & Peticolas, W. L. The internal dynamics of globular protein. *Critical Reviews in Biochemistry* **9**, 293-349 (1981).

91 Maffeo, C., Bhattacharya, S., Yoo, J., Wells, D. & Aksimentiev, A. Modeling and simulation of ion channels. *Chemical reviews* **112**, 6250-6284 (2012).

92 VanSchouwen, B., Akimoto, M., Sayadi, M., Fogolari, F. & Melacini, G. Role of dynamics in the autoinhibition and activation of the hyperpolarization-activated cyclic nucleotide-modulated (HCN) ion channels. *Journal of Biological Chemistry* **290**, 17642-17654 (2015).

93 Zhou, L. & Siegelbaum, S. A. Gating of HCN channels by cyclic nucleotides: residue contacts that underlie ligand binding, selectivity, and efficacy. *Structure* **15**, 655-670 (2007).

94 Berrera, M., Pantano, S. & Carloni, P. cAMP Modulation of the cytoplasmic domain in the HCN2 channel investigated by molecular simulations. *Biophysical journal* **90**, 3428-3433 (2006).

95 Giorgetti, A., Carloni, P., Mistrik, P. & Torre, V. A homology model of the pore region of HCN channels. *Biophysical journal* **89**, 932-944 (2005).

96 Kasimova, M. A. *et al*. Helix breaking transition in the S4 of HCN channel is critical for hyperpolarization-dependent gating. *Elife* **8** (2019).

97 Napolitano, L. M. R. *et al*. A structural, functional, and computational analysis suggests pore flexibility as the base for the poor selectivity of CNG channels. *Proceedings of the National Academy of Sciences* **112**, E3619-E3628 (2015).

98 Shi, C. *et al*. A single NaK channel conformation is not enough for non-selective ion conduction. *Nature communications* **9**, 1-8 (2018).

99 DeMarco, K. R., Bekker, S. & Vorobyov, I. Challenges and advances in atomistic simulations of potassium and sodium ion channel gating and permeation. *The Journal of physiology* **597**, 679-698 (2019).

100 Van Gunsteren, W. F. & Berendsen, H. J. A leap-frog algorithm for stochastic dynamics. *Molecular Simulation* **1**, 173-185 (1988).

101 Feller, S. E., Zhang, Y., Pastor, R. W. & Brooks, B. R. Constant pressure molecular dynamics simulation: the Langevin piston method. *The Journal of chemical physics* **103**, 4613-4621 (1995).

102 Parrinello, M. & Rahman, A. Polymorphic transitions in single crystals: A new molecular dynamics method. *Journal of Applied physics* **52**, 7182-7190 (1981).

103 Jorgensen, W. L., Chandrasekhar, J., Madura, J. D., Impey, R. W. & Klein, M. L. Comparison of simple potential functions for simulating liquid water. *The Journal of chemical physics* **79**, 926-935 (1983).

104 Zheng, L., Alhossary, A. A., Kwoh, C.-K. & Mu, Y. Molecular dynamics and simulation. (2019).

105 Phillips, J. C. *et al*. Scalable molecular dynamics with NAMD. *Journal of computational chemistry* **26**, 1781-1802 (2005).

106 Case, D. A. *et al*. The Amber biomolecular simulation programs. *Journal of computational chemistry* **26**, 1668-1688 (2005).

107 Klauda, J. B. *et al*. Update of the CHARMM all-atom additive force field for lipids: validation on six lipid types. *The journal of physical chemistry B* **114**, 7830-7843 (2010).

108 Felts, A. K., Gallicchio, E., Wallqvist, A. & Levy, R. M. Distinguishing native conformations of proteins from decoys with an effective free energy estimator based on the opls all-atom force field and the surface generalized Born solvent model. *Proteins: Structure, Function, and Bioinformatics* **48**, 404-422 (2002).

109 Oostenbrink, C., Soares, T. A., Van der Vegt, N. F. & Van Gunsteren, W. F. Validation of the 53A6 GROMOS force field. *European Biophysics Journal* **34**, 273-284 (2005).